

## **Chapter 2**

# **Contribution of First- versus Second-Generation Products to Secondary Organic Aerosols Formed in the Oxidation of Biogenic Hydrocarbons\***

---

\*This chapter is reproduced by permission from “Contribution of first- versus second-generation products to secondary organic aerosols formed in the oxidation of biogenic hydrocarbons” by N. L. Ng, J. H. Kroll, M. D. Keywood, R. Bahreini, V. Varutbangkul, R. C. Flagan, J. H. Seinfeld, A. Lee., and A. H. Goldstein, *Environmental Science and Technology*, 40, 2283-2297, 2006. Copyright 2006. American Chemical Society.

## 2.1 Abstract

Biogenic hydrocarbons emitted by vegetation are important contributors to secondary organic aerosol (SOA), but the aerosol formation mechanisms are incompletely understood. In this study, the formation of aerosols and gas-phase products from the ozonolysis and photooxidation of a series of biogenic hydrocarbons (isoprene, 8 monoterpenes, 4 sesquiterpenes and 3 oxygenated terpenes) are examined. By comparing aerosol growth (measured by Differential Mobility Analyzers, DMAs) and gas-phase concentrations (monitored by a Proton Transfer Reaction Mass Spectrometer, PTR-MS), we study the general mechanisms of SOA formation. Aerosol growth data are presented in terms of a “growth curve”, a plot of aerosol mass formed versus the amount of hydrocarbon reacted. From the shapes of the growth curves, it is found that all the hydrocarbons studied can be classified into two groups based entirely on the number of double bonds of the hydrocarbon, regardless of the reaction systems (ozonolysis or photooxidation) and the types of hydrocarbons studied: compounds with only one double bond and compounds with more than one double bond. For compounds with only one double bond, the first oxidation step is rate-limiting and aerosols are formed mainly from low volatility first-generation oxidation products; whereas for compounds with more than one double bond, the second oxidation step may also be rate-limiting and second-generation products contribute substantially to SOA growth. This behavior is characterized by a vertical section in the growth curve, in which continued aerosol growth is observed even after all the parent hydrocarbon is consumed.

## 2.2 Introduction

Organic aerosols are a significant contributor to the total particulate matter in the troposphere, and a full understanding of their sources and properties is necessary to evaluate their impacts on visibility, climate, and human health. Secondary organic aerosols (SOA), formed from production of low-volatility species from the oxidation of gas-phase organic compounds, contribute a significant fraction of fine particulate matter, as high as 50-80 % in polluted regions (1).

The oxidation of biogenic non-methane hydrocarbons (NMHCs) emitted by vegetation, such as isoprene ( $C_5H_8$ ), monoterpenes ( $C_{10}H_{16}$ ), sesquiterpenes ( $C_{15}H_{24}$ ) and oxygenated terpenes (e.g.  $C_{10}H_{18}O$ ,  $C_{10}H_{12}O$ ) are especially important to the total atmospheric burden of SOA. Because of their large global emissions and high reactivity with the major atmospheric oxidants, ozone ( $O_3$ ), hydroxyl radical (OH) and nitrate radical ( $NO_3$ ) (2), they are believed to be the dominant contributors to global SOA formation (3).

Despite considerable study of the oxidation mechanisms of these biogenic compounds (4-16), the basic underlying mechanisms of SOA formation and growth from biogenic precursors remain poorly understood. Numerous gas-phase and aerosol-phase oxidation products have been identified, but carbon balances are poorly constrained and the formation mechanisms for such products remain speculative. With the possibility of multiple oxidation steps, a particular condensable compound may be formed by the direct oxidation of the parent hydrocarbon, or through the further oxidation of first-generation gas-phase products (7, 17-24). In addition, the formation of oligomers in SOA adds complexity to the overall SOA forming reaction mechanism (25-29). Furthermore, it is

unclear whether the rate-determining step to SOA formation is the first oxidation step or the further oxidation steps (in either the gas or aerosol phase). Identifying the rate-determining step can certainly constrain the SOA formation mechanisms, as well as provide the important kinetic information in modeling SOA formation.

Laboratory-determined SOA yield, defined as the ratio of the mass concentration of aerosol formed to that of the hydrocarbon reacted, is widely used as a quantitative measure of the SOA-forming potential of a parent hydrocarbon. The aerosol yield may be described by a semi-empirical model developed by Odum et al. (30) based on absorptive gas-particle partitioning (31, 32) of two reaction products, representing compounds of differing volatility:

$$Y = \Delta M_o \left[ \frac{\alpha_1 K_{om,1}}{1 + K_{om,1} \Delta M_o} + \frac{\alpha_2 K_{om,2}}{1 + K_{om,2} \Delta M_o} \right] \quad (2.1)$$

in which  $Y$  is the aerosol yield,  $\Delta M_o$  is the organic aerosol mass produced,  $\alpha_i$  is the mass-based gas-phase stoichiometric fraction for species  $i$ , and  $K_{om,i}$  is the gas-particle partitioning coefficient for species  $i$ . With this two-product model, equation (2.1) can be fit to experimental yield data to determine values for  $\alpha_i$  and  $K_{om,i}$ , and the resulting plot ( $Y$  versus  $\Delta M_o$ ) is generally referred to as a “yield curve”. Over the years, yield curves have proven to be useful in representing SOA formation (9, 17, 30, 33-36), allowing the contribution of SOA to the particulate burden in the atmosphere to be estimated, even when the detailed SOA component speciation is not available (37).

Recently it has been shown that this model may be used for the interpretation of laboratory SOA growth data in terms of underlying chemistry (38, 39). By rewriting  $Y$  in

equation (2.1) as  $\Delta M_o/\Delta HC$  and assuming no absorbing organic aerosol is present initially, an expression for  $\Delta M_o$  as a function of  $\Delta HC$  may be obtained:

$$\Delta M_o = \frac{1}{2} \left( \Delta HC(\alpha_1 + \alpha_2) - \frac{1}{K_{om,1}} - \frac{1}{K_{om,2}} \right) + \frac{\sqrt{4K_{om,1}K_{om,2}(K_{om,1}\alpha_1\Delta HC + K_{om,2}\alpha_2\Delta HC - 1) + (K_{om,1} + K_{om,2} - K_{om,1}K_{om,2}\Delta HC(\alpha_1 + \alpha_2))^2}}{2K_{om,1}K_{om,2}} \quad (2.2)$$

As written, equations (2.1) and (2.2) are only valid when there is no absorbing organic mass present initially and that the absorbing medium is produced completely by the oxidation of the parent hydrocarbon. In the above equations,  $\Delta M_o$  is defined as  $M_o - M_{o,initial}$ . For chamber experiments, there is no absorbing organic mass present initially and so  $M_{o,initial} = 0$  and  $\Delta M_o = M_o$ . By plotting experimentally measured aerosol growth,  $\Delta M_o$ , as a function of the amount of hydrocarbon reacted,  $\Delta HC$  (hereafter referred to as a “growth curve”), it is found that the effects of heterogeneous chemistry and gas-phase reactions of oxidation products can be inferred (38). For example, it is clear that secondary reactions (further oxidation of first-generation products) play an important role in SOA growth for the oxidation of both biogenic and anthropogenic precursors (7, 17-19); however, the relative contribution of first- and second-generation products to SOA formation and growth is still unclear.

It has been generally assumed that both the yield curve expression (equation 2.1) and growth curve expression (equation 2.2) are only valid for the final SOA growth, i.e. the amount of SOA formed once the hydrocarbon is all reacted, gas-particle equilibrium is established and aerosol growth has completed. Therefore, a series of experiments with different initial hydrocarbon concentrations have traditionally been carried out for each

parent hydrocarbon to establish the yield curve/growth curve. However, one can still plot the growth curve for a single experiment over the course of the experiment (the “time-dependent growth curve”). Time-dependent aerosol formation and growth data have been examined in a few studies (7, 17, 19, 39); however, it has not been established whether it is appropriate to use time-dependent growth data to understand SOA formation in terms of the equilibrium expressions above.

In this study, the SOA formation and gas-phase oxidation products from the ozonolysis and photooxidation of a series of biogenic compounds are investigated. Overall SOA yields, gas-phase oxidation products and yields, as well as detailed multistep oxidation mechanisms from these experiments are presented in Lee et al. (20, 21). Many of these oxidation products have been observed in the Ponderosa pine canopy at Blodgett Forest in California (40). The focus here is the general mechanisms of SOA growth. By comparing gas-phase concentrations and aerosol volume in real time over the course of each experiment, we are able to study the kinetics and mechanisms of SOA formation. In particular, we focus on the contribution of secondary reactions to SOA growth in both the ozonolysis and photooxidation systems, by constructing a time-dependent growth curve for each experiment. The shapes of the growth curves reveal clearly the importance and the relative contribution of secondary reactions to SOA growth in different systems. We show that the biogenic hydrocarbons studied can be classified into two main groups based on the number of double bonds of the parent hydrocarbon. For compounds with only one double bond, the first oxidation step is the rate-determining step, and SOA is formed from the condensation of first-generation products. However, for compounds with more than one double bond, the further

oxidation of first-generation products appears to be rate-determining as well, and secondary reactions contribute substantially to SOA growth.

### 2.3 Experimental

Experiments are performed in Caltech's indoor, dual 28 m<sup>3</sup> Teflon environmental chambers. Details of the facilities have been described elsewhere (36, 41) so will only be described briefly here. Before each experiment, the chambers are flushed continuously with purified air for ~32 hours.

Each chamber has a dedicated Differential Mobility Analyzer (DMA, TSI model 3081) coupled with a condensation nucleus counter (TSI model 3760) for measuring aerosol size distribution, number concentration, and total volume. Separate CPCs (TSI models 3010 and 3025) are used to monitor the total number of particles in each chamber as an additional check. All aerosol growth data are corrected for wall loss, in which size-dependent coefficients are determined from wall loss experiments and applied to the aerosol volume data (36). Temperature and relative humidity (RH) are continuously monitored using combined temperature and RH probes (Vaisala HMP233 series transmitters, Woburn, MA).

For experiments with isoprene, monoterpenes, and oxygenated terpenes, seed aerosols are introduced into the chamber to act as a substrate onto which the gas-phase products may condense. Seed aerosols are generated by atomizing an aqueous ammonium sulfate solution with a constant-rate atomizer. The aerosol stream is passed through two <sup>210</sup>Po neutralizers to reduce charges and minimize loss in the lines. The initial particle number concentration is about 20,000 particles cm<sup>-3</sup>, with a geometric mean diameter of 80-100 nm. Sesquiterpenes react with ozone and OH radicals at sufficiently fast rates that

nucleation occurs despite the presence of seed aerosols, resulting in two modes (nucleation mode and condensation mode), making data analysis (particularly the wall loss calculation) difficult. Thus, for sesquiterpene experiments no seed particles are added.

After atomization, a known volume of the parent hydrocarbon is injected into a glass bulb, and introduced into the chambers by gentle heating. The concentration of the parent hydrocarbons is monitored using two instruments, a Hewlett Packard gas chromatograph with flame ionization detection, GC-FID (Hewlette-Packard, 5890), and a Proton Transfer Reaction Mass Spectrometer, PTR-MS (Ionicon Analytik, Innsbruck, Austria) (42). The PTR-MS calibrations and measurements are described in more detail in Lee et al. (20, 21). The PTR-MS monitors concentrations of both the parent hydrocarbon and various gas-phase intermediates and products continuously over the course of the experiments. The PTR-MS is operated in mass scan mode, with each cycle completed in ~3 minutes; this time scale is much shorter than that of the GC-FID, allowing the evolution of gas-phase products to be well-captured. Together, the PTR-MS and DMA allow for simultaneous measurements of gas-phase product concentrations and aerosol growth. Aerosol mass and chemical composition are monitored with an Aerodyne quadrupole aerosol mass spectrometer (AMS). Details on the operation of AMS and its data analysis have been described elsewhere (43-46). The hygroscopicity of the aerosol is measured by a Tandem Differential Mobility Analyzer (TDMA).

For ozonolysis experiments, the temperature of the chamber is maintained at 20°C and the RH is <10%. Seed aerosols are generated by atomizing a 0.03 M (NH<sub>4</sub>)<sub>2</sub>SO<sub>4</sub> solution. The particles also pass through a silica gel diffusion dryer before they enter the



chamber. Cyclohexane is used to scavenge OH radicals formed from the hydrocarbon-O<sub>3</sub> reaction and to ensure ozone is the only oxidant present in the chamber. Enough cyclohexane is injected such that the reaction rate of OH radicals with cyclohexane is 100 times greater than that with parent hydrocarbon. Once the chamber contents are well mixed and GC-FID and PTR-MS readings are stabilized, ozone is injected into the chambers at 5 L min<sup>-1</sup>. Ozone is generated with a UV lamp ozone generator (EnMet Corporation, MI). The amount of ozone injected is 3 times the concentration of the parent hydrocarbon. Ozone concentration is measured by a commercial ozone monitor (Horiba APOA-360 CE, Irvine, CA). The beginning of ozone injection marks the start of each experiment.

For several  $\alpha$ -pinene ozonolysis experiments, the experimental conditions are slightly different, as described by Gao et al. (27, 28). Those experiments are carried out at ~55% RH by passing dry purified air through a bubbler prior to introduction into the chamber. The seed particles are generated by atomizing a 0.03 M MgSO<sub>4</sub> solution and they are not passed through the diffusion dryer prior to introduction into the chamber. Ozone is injected at twice the concentration of the parent hydrocarbon. Hydrocarbon concentration is monitored by GC-FID only.

For photooxidation studies, the experiments are conducted at 20-22°C and ~50% RH. Seed particles are generated by atomizing a 0.015 M aqueous (NH<sub>4</sub>)<sub>2</sub>SO<sub>4</sub> solution. For isoprene and monoterpenes, the parent hydrocarbon concentration is measured by both GC-FID and PTR-MS, while only PTR-MS is used for experiments with sesquiterpenes and oxygenated terpenes. After injection of seed (for the isoprene, monoterpene and oxygenated terpene experiments) and parent hydrocarbon, the OH

precursor, nitrous acid (HONO), is introduced. HONO is prepared by dropwise addition of 2 mL of 1% NaNO<sub>2</sub> into 15 mL of 10% H<sub>2</sub>SO<sub>4</sub> in a glass bulb. The bulb is then attached to the chamber and a stream of dry air is passed through the bulb, introducing HONO into the chamber. NO and NO<sub>2</sub>, measured by a commercial NO<sub>x</sub> monitor (Horiba APNA-360, Irvine, CA), form as side products in the preparation of HONO, and are also introduced into the chamber. HONO is observed by PTR-MS as the dehydrated form of HONOH<sup>+</sup> at *m/z* 30, and also appears to be detected by the NO<sub>x</sub> monitor. However, since HONO calibration is not performed, its concentration in the chamber is not well-constrained.

Once the seed, parent hydrocarbon, and NO<sub>x</sub> concentrations have stabilized, reaction is initiated by irradiating the chamber with blacklights. The blacklights used are centered at 354 nm, efficiently photolyzing HONO to OH and NO. Only 10% of the lights are used to minimize temperature increases. Over the course of the experiments, the temperature of the chambers increases by only 1-2°C and RH drops accordingly. However, RH never drops below 40%, the efflorescence RH of ammonium sulfate.

The chemicals used and their stated purities are: isoprene (Aldrich, 99.8%), α-pinene (Aldrich, ≥99%), β-pinene (Fluka, ≥99%), Δ<sup>3</sup>-carene (Aldrich, 99%), α-terpinene (Fluka, ≥97%), γ-terpinene (Fluka, ≥98.5%), terpinolene (Fluka, ≥97%), limonene (Aldrich, 97%), myrcene (Fluka, 90%), α-humulene (Sigma, purity not specified), β-caryophyllene (Aldrich, purity not specified), aromadendrene (Fluka, ≥97%), longifolene (Fluka, ≥99%), methyl chavicol (Fluka, ≥98.5%), verbenone (Fluka, 99%), and linalool (Fluka, 97%).

Table 2.1 lists the structures of the parent hydrocarbons studied and the rate constants of the compounds for reaction with ozone ( $k_{\text{ozone}}$ ) and OH radicals ( $k_{\text{OH}}$ ). The experimental conditions for ozonolysis and photooxidation experiments are given in Tables 2.2 and 2.3 respectively.

## 2.4 Results

### 2.4.1 Ozonolysis studies

The compounds studied in the ozonolysis experiments are  $\alpha$ -pinene,  $\beta$ -pinene,  $\Delta^3$ -carene,  $\alpha$ -terpinene, terpinolene, myrcene,  $\alpha$ -humulene,  $\beta$ -caryophyllene, methyl chavicol, and linalool. Once ozone is introduced into the chamber, the parent hydrocarbon concentration is observed to decay, and various gas-phase oxidation products are formed accordingly. SOA growth typically begins within 30 minutes after reaction initiation, except for methyl chavicol, in which no SOA growth is observed until an hour after ozone injection. No significant SOA growth is observed from linalool ozonolysis. By comparing volume distributions from the DMA and mass distributions from the AMS, the effective densities for the SOA formed in ozonolysis may be estimated (46). Overall, an average effective density of  $1.25 \text{ g cm}^{-3}$  is used to convert the total aerosol volume measured by DMA to total mass for both ozonolysis and photooxidation experiments.

A typical reaction profile for  $\alpha$ -pinene ozonolysis is shown in Figure 2.1. This profile exemplifies that for all parent compounds with a single double bond. Once ozone is injected,  $\alpha$ -pinene begins to be oxidized, its concentration decreases, and the aerosol mass starts to increase. Aerosol growth reaches its maximum when all  $\alpha$ -pinene is

consumed and remains constant thereafter. A typical reaction profile for terpinolene is shown in Figure 2.2; terpinolene exemplifies the behavior of compounds with more than one double bond. Unlike  $\alpha$ -pinene, in which aerosol growth stops at the time when the hydrocarbon is consumed, the aerosol mass generated in the ozonolysis of terpinolene reaches its maximum well after the terpinolene is completely consumed (this will be discussed further in Section 2.5.2.3). The SOA growth in the ozonolysis studies is seen more directly by plotting organic aerosol mass as a function of the hydrocarbon reacted over the course of the experiment (time-dependent growth curve). The time-dependent growth curves for all compounds studied in ozonolysis experiments (except linalool, which does not produce significant SOA) are shown in Figure 2.3.

#### **2.4.2 Photooxidation studies**

In the photooxidation experiments, initiated by the irradiation of hydrocarbon/HONO/NO<sub>x</sub> mixtures, the OH radical is the dominant oxidant. Ozone and NO<sub>3</sub> radicals are also formed during the experiments, so their chemistry may play a role as well. Based on the decay of the parent hydrocarbon and the measured ozone level in the chamber, O<sub>3</sub> and NO<sub>3</sub> account only for a very small fraction of the parent hydrocarbon consumption; however, we cannot rule out the possible role of O<sub>3</sub> or NO<sub>3</sub> reactions with the oxidation products. The compounds studied in the photooxidation experiments are isoprene,  $\alpha$ -pinene,  $\beta$ -pinene,  $\Delta^3$ -carene,  $\alpha$ -terpinene,  $\gamma$ -terpinene, limonene, terpinolene, myrcene,  $\alpha$ -humulene,  $\beta$ -caryophyllene, aromadendrene, longifolene, methyl chavicol, verbenone, and linalool. Once the chamber irradiation begins, the hydrocarbon concentration decreases and various gas-phase products are formed accordingly. SOA growth typically begins 10 minutes after reaction initiation.

The time-dependent growth curves for the compounds studied (except longifolene, discussed subsequently) are shown in Figure 2.4.

## 2.5 Discussion

Based on Figures 2.3 and 2.4, we can classify all the compounds studied into two different groups based entirely on the shapes of the growth curves: compounds for which SOA growth stops once all the parent hydrocarbon is consumed, and compounds for which SOA growth continues even after all the hydrocarbon is consumed. The latter case is characterized by a vertical section in the growth curves. Such classifications are independent of the reaction system studied (ozonolysis or photooxidation) as well as the class of compounds studied (isoprene, monoterpene, sesquiterpene or oxygenated terpene). All compounds in the first group have one double bond while compounds in the second group have more than one double bond.

The first group of compounds includes  $\alpha$ -pinene,  $\beta$ -pinene,  $\Delta^3$ -carene, aromadendrene, longifolene, methyl chavicol, and verbenone. The fact that aerosol growth stops once all hydrocarbon is consumed indicates that the first oxidation reaction is the rate-determining step in SOA formation. In this case, either the condensable products are the initial reaction products of the parent hydrocarbon oxidation (first-generation products), or subsequent reactions (in either the gas or aerosol phase) also contribute to aerosol growth, but proceed at very fast rates.

The second group of compounds includes isoprene,  $\alpha$ -terpinene,  $\gamma$ -terpinene, limonene, terpinolene, myrcene,  $\alpha$ -humulene,  $\beta$ -caryophyllene, and linalool. For these compounds, the growth curve can be divided into two regions. We can see that more SOA is formed as the parent hydrocarbon reacts (region I). Even after all the hydrocarbon

is completely consumed, aerosol mass continues to increase, resulting in a vertical section of the growth curve (region II). The delay in aerosol production for this group of compounds may be a result of either of the following two factors: there is delay in mass transfer, in which the partitioning of condensable products into the aerosol phase is extremely slow, or condensable products are formed from the further oxidation of first-generation products, and this second oxidation step also determines the rate of SOA formation. However, a delay in mass transfer is not observed for all compounds with only one double bond, hence it seems unlikely that SOA formation for compounds with more than one double bond will be mass-transfer limited. For this group of compounds, the first-generation products formed are still unsaturated, thus will react further with the oxidants (OH, O<sub>3</sub> or NO<sub>3</sub>) to yield compounds more highly oxidized than the first-generation products. As a result, for this group of compounds there are significant contributions from secondary reactions to SOA growth. In many cases, good correlations exist between the extent to which intermediate gas-phase products react and aerosol growth; these will be discussed subsequently. There is a possibility that the first step is rate-limiting, and the second step is fast and only the second step leads to SOA growth, then the growth curve will look like compounds with only one double bond (i.e. no vertical section). However, for all the 9 compounds with more than one double bond we have studied, we found that all the growth curves exhibit a vertical section. Therefore, this scenario is unlikely to be the case, and for compounds with more than one double bond, both oxidation steps are rate-limiting, allowing one to infer the importance of the different generation products based upon these kinetic arguments.

In the following sections, the two classes of compounds will be examined in greater detail. We select one compound from each class:  $\alpha$ -pinene ozonolysis as a representative of SOA formation from compounds with one double bond and terpinolene ozonolysis as representing the behavior of compounds with more than one double bond. The time-dependent growth curves and final SOA concentrations for each system will be discussed. From the shapes of the growth curves of these two systems, two different general SOA formation mechanisms can be inferred. Based on this analysis, we will discuss the underlying chemistry of SOA formation of individual compounds.

## **2.5.1 Time-dependent vs. final SOA growth**

### **2.5.1.1 $\alpha$ -pinene ozonolysis (one double bond)**

Substantial insight can be gained by examining time-dependent SOA growth over a range of hydrocarbon concentrations. Here we re-examine  $\alpha$ -pinene ozonolysis experiments previously reported by Gao et al. (27, 28). The data set includes 7  $\alpha$ -pinene ozonolysis experiments, with initial  $\alpha$ -pinene concentrations ranging from 12 to 135 ppb. These experiments were carried out at slightly different reaction conditions than those shown in Figures 2.3 and 2.4, as described in the Experimental section.

Based on the final SOA growth data from these 7  $\alpha$ -pinene experiments, a yield curve may be generated using the two-product model derived by Odum et al. (30, 33), and converted to a growth curve by using equation (2.2). For clarification, this growth curve is referred to as the “final SOA growth curve” as each data point represents the final aerosol mass resulting from the complete oxidation of a certain amount of parent hydrocarbon. The time-dependent growth curves from these experiments are shown

together with the final SOA growth curve in Figure 2.5. It can be seen that the individual data points for each  $\alpha$ -pinene experiment overlap remarkably well not only with each other, but also with the final SOA growth curve, suggesting that for compounds with only one double bond such as  $\alpha$ -pinene, both equations (2.1) and (2.2) are valid for the final SOA growth as well as the time-dependent growth data. It also suggests that the chemical composition of the aerosol remains essentially constant over the course of the oxidation. This constancy is confirmed by AMS measurements; it has been shown through delta series analysis of mass spectra that one can obtain information about the general oxidation state of particle-phase compounds (46). It is observed that unsaturated organics yield delta values  $\leq 0$  while oxygenated organics yield delta values  $\geq 2$  (46, 47). The delta values over the course of an  $\alpha$ -pinene experiment are shown in Figure 2.6. The different delta values stay relatively constant after the reaction starts, suggesting no substantial changes in the degree of oxidation of SOA composition over time. This observation is also in agreement with the study by Yu et al. (7), who found that the time-dependent yield curve agrees well with that generated by experimentally determined  $\alpha_i$  and  $K_{om,i}$ , which are obtained from the analysis of the denuder/filter samples collected at the end of the experiment.

### **2.5.1.2 Terpinolene ozonolysis (more than one double bond)**

For behavior characteristic of SOA formation from a precursor hydrocarbon with more than one double bond, we examine the terpinolene ozonolysis experiments reported previously by Keywood et al. (36) (the experiment on 3/31/03 in Table 2 of Keywood et al. is the same as that shown in Figure 2.2 of this paper). We note that the yields reported in Keywood et al. (36) are based on GC-FID measurements, which are typically 10-15%



higher than those based on PTR-MS measurements; since we use mainly PTR-MS for gas-phase measurements here, we scale up accordingly the parent hydrocarbon concentrations for those experiments in which only GC-FID was used. We have recalculated the aerosol yields for these 8 experiments, obtaining a new set of aerosol yield parameters for the two-product model:  $\alpha_1 = 0.243$ ,  $\alpha_2 = 0.03$ ,  $K_{om,1} = 0.014$  and  $K_{om,2} = 0.927$ . This scaling changes the parameters from Keywood et al. (36) only slightly, and has no effect on the conclusions from either work.

Shown in Figure 2.7 are the time-dependent growth data for the 8 terpinolene ozonolysis experiments, together with the growth curve based on the final data for each experiment. Unlike the case for  $\alpha$ -pinene (Figure 2.5), the time-dependent growth curves and final SOA growth curve for terpinolene are all dramatically different. While the time-dependent growth curves for individual experiments clearly show the contribution of the secondary reactions, this information is not evident by considering just the final SOA growth curve. Therefore, in the case when secondary reactions play a role in SOA production, one cannot use the time-dependent growth data from a single experiment to represent final growth conditions. Moreover, the time-dependent growth curve for a single experiment cannot be fitted to the two-product model, indicating that for compounds with more than one double bond, this model is valid only when the data represent final SOA growth, when all the hydrocarbon is reacted, secondary reactions are complete and gas-particle equilibrium is reached.

Using  $\alpha$ -pinene and terpinolene as model systems, we now extend our analysis to other compounds to study the underlying mechanisms of SOA formation.

## 2.5.2 Chemistry of individual compounds

### 2.5.2.1 $\alpha$ -pinene ozonolysis

The growth curves of  $\alpha$ -pinene ozonolysis and photooxidation indicate that in these systems the first oxidation step is the rate-determining step as aerosol growth stops when the hydrocarbon is completely consumed. In these systems SOA is formed from the condensable first-generation products. The identification of the rate-determining step and that SOA are formed from first-generation products allow us to constrain the reaction mechanism substantially.

Much effort has been expended in identifying the oxidation products of  $\alpha$ -pinene ozonolysis and a number of organic acids have been identified as major products: oxocarboxylic acids (pinonic acid and norpinonic acid), dicarboxylic acids (pinic acid and norpinic acid), and hydroxy pinonic acid (4-8, 10-12). According to Yu et al. (7), these compounds account for about 73% of the total aerosol mass. Different mechanisms leading to the formation of organic acids have been proposed. Pinonic acid is generally thought to be a first-generation product, either by rearrangement of a Criegee intermediate to a carboxylic acid (4, 10, 48), or by reaction of the stabilized Criegee intermediates with water (6, 49). Most studies suggest that other acids are formed from the further oxidation of their corresponding aldehydes (4, 6, 10, 12, 48). In our ozonolysis experiments, OH radicals are scavenged by cyclohexane, and so ozone is the only gas-phase oxidant. It is found that the molar ratio of ozone consumed to  $\alpha$ -pinene reacted is 1:1, suggesting that ozone reacts only with the parent hydrocarbon and that there are no further oxidation steps in the gas phase. These data indicate that the ozone-alkene reaction is the rate-determining step, and that the condensable products are first-

generation products. Thus, mechanisms speculating that acids are formed by multiple oxidation steps in the gas phase are not consistent with the data. Our study does not exclude the formation of individual components of SOA through heterogeneous reactions; however, it would suggest that these reactions, if they do contribute to aerosol growth on the timescale of our experiments, proceed at very fast rates. The PTR-MS data show that the pinonaldehyde concentration stays constant after  $\alpha$ -pinene is completely consumed (Figure 2.8), indicating that pinonaldehyde is not further oxidized to form significant amounts of condensable products, and that it is unlikely to be involved in heterogeneous reactions (such as oligomerization) to contribute substantially to additional aerosol mass as suggested by Tolocka et al. (25) and Iinuma et al. (26). On the other hand, mechanisms involving formation of organic acids as first-generation reaction products, such as those put forth by Jenkin et al. (49) for pinic acid and hydroxyl pinonic acid, are consistent with the data.

#### **2.5.2.2 $\alpha$ -pinene photooxidation**

As in the case of ozonolysis, for the photooxidation of  $\alpha$ -pinene, carboxylic acids have been found to be predominant in the aerosol phase (13-16). Most suggested mechanisms involve multiple oxidation steps; for example, the oxidation of pinonaldehyde may form pinonic acid, which could then react further to form pinic and norpinic acids (13, 15, 16). In the present experiments, pinonaldehyde is indeed observed to decrease when  $\alpha$ -pinene is almost completely consumed (Figure 2.9), likely a result of reaction with OH and photodissociation (50). However, the loss of pinonaldehyde is not accompanied by further aerosol growth, so the formation of low volatility organic acids through the further oxidation of pinonaldehyde seems unlikely. This is consistent with the

observation by Hatakeyama et al. (51), in which the pinonaldehyde yield and SOA yield are not well-correlated. Therefore, the acids are likely formed as first-generation products, as suggested by Larsen et al. (13), or else by oxidation reactions of species already in the particle phase.

### 2.5.2.3 Terpinolene ozonolysis

The growth curve for terpinolene ozonolysis indicates that the further oxidation of first-generation products contributes significantly to SOA growth and that the second oxidation step may also be rate-limiting. Unlike the case for  $\alpha$ -pinene ozonolysis, ozone concentration is observed to decrease even after all the terpinolene is consumed, indicating there is further alkene oxidation. The PTR-MS measures the concentrations of different gas-phase products over the course of the each experiment, including some of the first-generation oxidation products. From the time evolution of these first-generation products, aerosol growth can be correlated with the further oxidation of these products. The time evolution of two intermediate ions ( $m/z$  111 and  $m/z$  93), corresponding to first-generation oxidation products (of mass 110 and 92 amu) is shown in Figure 2.10. At  $t \cong 50$  min, all the terpinolene is consumed and yet the aerosol growth continues, with a slightly different rate (This difference in the rate of aerosol growth is much more pronounced in the case for  $\beta$ -caryophyllene, which is discussed below). As shown in Figure 2.10, both the  $m/z$  111 and  $m/z$  93 peaks start to decrease when terpinolene is totally consumed. The similar time evolution of these compounds and the 18 amu difference suggests that the  $m/z$  93 ion is a dehydrated fragment of the  $m/z$  111 ion (20). The  $m/z$  111 peak is likely to be the protonated form of 4-methyl-3-cyclohexen-1-one (MW=110), known to be a major product of terpinolene ozonolysis (52, 53). The molar

yield of this product (taken from summing the calculated yields from  $m/z$  111 and  $m/z$  93) is 0.53. Based on this molar yield, we can calculate the amount of the product formed over the course of the experiment, and from the time-dependent PTR-MS data we can estimate the amount reacted away over time; these are shown in Figure 2.11. Figure 2.12 shows the SOA mass formed as a function of the amount of the intermediate product reacted. There is a clear correlation between the two, suggesting a contribution from the further oxidation of the intermediate product to the SOA formed. The intercept corresponding to the amount of aerosol mass already formed before any of the first-generation product has reacted away, is  $\sim 70 \mu\text{g m}^{-3}$ . This is similar to the amount of SOA formed before terpinolene is fully consumed (Figure 2.3). We do not quantify the contribution of second-generation products to total SOA growth, as this percentage is likely to be a function of the amount of organic matter present. Nevertheless, we can still infer from these results that a large fraction of SOA produced is from second-generation chemistry.

The remainder of the SOA formed is mostly from the condensation of relatively nonvolatile first-generation products (in the first 50 minutes of the experiment), likely from the attack of ozone on the endo-double bond, which results in larger, multifunctional molecular weight products. Only when terpinolene is completely consumed does the reaction of relatively volatile first-generation species with ozone become important. For terpinolene, it appears that the reaction of the intermediate corresponding to the  $m/z$  111 ion (likely 4-methyl-3-cyclohexen-1-one) is largely responsible for this additional aerosol growth. We do not observe a correlation between the decay of other products and aerosol growth.

#### 2.5.2.4 Terpinolene and limonene photooxidation

As in the ozonolysis case, for terpinolene photooxidation, we observe the  $m/z$  111 and  $m/z$  93 ions start to decrease when the parent hydrocarbon is consumed; again the same time evolution of these two products suggests that the  $m/z$  93 ion is the dehydrated fragment of  $m/z$  111. These are likely to correspond to the same compound, 4-methyl-3-cyclohexen-1-one, a known product of the OH+terpinolene reaction (52, 53). We measure the total molar yield to be 0.47 (sum of the molar yields from the  $m/z$  93 and  $m/z$  111 ions). Aerosol growth as a function of the amount of the  $m/z$  111 ion reacted is shown in Figure 2.13. Again a good correlation is observed, suggesting the further oxidation of 4-methyl-3-cyclohexen-1-one contributes to aerosol growth in the photooxidation system.

The photooxidation of limonene, which is structurally similar to terpinolene, shows a substantially lower contribution from secondary products to total SOA formed. The major product ion observed to decrease when limonene is almost all consumed is  $m/z$  169, likely to be limononaldehyde (MW=168) (52). Limononaldehyde is not calibrated in the PTR-MS, however, by analogy to the fragmentation of pinonaldehyde, limononaldehyde can be expected to fragment not only at  $m/z$  151, the dehydrated fragment of  $m/z$  169, but also at  $m/z$  107, 123, 133, and 151, with a molar yield of 0.61 from the sum of all limononaldehyde-associated ions and their isotopes. The correlation of the  $m/z$  169 ion (including the fragmented ions and isotopes) reacted and aerosol growth is shown in Figure 2.14.

Differences in the vertical section of the growth curves indicate that secondary reactions contribute to SOA production to a larger extent in the case of terpinolene than

limonene. The large difference between the importance of secondary products from terpinolene and limonene can be explained in terms of their oxidation mechanisms, particularly the importance of oxidative attack on the exo versus endo double bonds. It is estimated that OH attack on the endo double bond accounts for only 44% of the OH-terpinolene reaction but 63% of the OH-limonene reaction (54), due to differing levels of alkyl substitution of each. As described above, the contribution of second-generation products to total SOA growth is smaller for limonene than for terpinolene. This suggests that the higher percentage of OH attack at the endo double bond results in more nonvolatile first-generation products, and hence a smaller contribution of second-generation products to total SOA formed. This is intuitive as radical attack at the endo double bond results in ring opening, forming multifunctional products with no loss of carbon. Hence, attack at the endo site is more likely to lead to the formation of condensable species. By contrast, attack at the exo double bond typically leads to fragmentation, reducing the number of carbons in the molecule and adding only one polar group. Hence the relative rates of attack at the endo and exo sites can play a major role in determining the importance of first versus second-generation products in SOA formation.

#### **2.5.2.5 Isoprene photooxidation**

It has recently been shown that isoprene photooxidation produces SOA in low yields under high  $\text{NO}_x$  conditions and that the SOA formation proceeds from the further reaction of first-generation products (55, 56). We can gain insights into the isoprene SOA formation mechanism by examining the growth curve of isoprene photooxidation as shown in Figure 2.4. It is clear that  $\sim 290 \mu\text{g m}^{-3}$  ( $\sim 100$  ppb) of isoprene has reacted before aerosol growth commences. This time delay in SOA formation, as well as the

continuous aerosol growth after isoprene is completely consumed, suggests that isoprene SOA is indeed a result of further oxidation of first-generation products and this step may also be rate-limiting. Methacrolein, a first-generation product of isoprene oxidation, can lead, upon photooxidation, to aerosol growth (55). Indeed, in Figure 2.15 it is shown that the total concentration of methacrolein and methyl vinyl ketone (which are isomers so cannot be distinguished in the PTR-MS) starts to decrease when isoprene is almost completely consumed. Shown in Figure 2.16 is the correlation between the amount of SOA formed and methacrolein + methyl vinyl ketone reacted. The plot has an intercept of  $4.8 \mu\text{g m}^{-3}$ , suggesting that this small amount of SOA is possibly formed from some more nonvolatile first-generation products and SOA is mainly formed from second-generation products. It has been shown that methyl vinyl ketone does not lead to aerosol growth (55), thus a large fraction of SOA growth is likely related to the oxidation of methacrolein.

#### **2.5.2.6 Other compounds with multiple double bonds**

Good correlations between aerosol growth and the amount of reacted intermediate products are also observed in the following systems: myrcene ozonolysis, myrcene photooxidation,  $\gamma$ -terpinene photooxidation, and linalool photooxidation. Tables 2.4 and 2.5 summarize the major first-generation products that are well-correlated with aerosol growth in these systems. Plots of aerosol growth versus the amount of reacted intermediates are presented in the Supporting Information. Other than the major first-generation products, certain products are also observed to decrease when the parent hydrocarbon is almost consumed; however, their concentrations are too low to obtain a



precise correlation between aerosol growth and the amount of these intermediates reacted.

For compounds such as  $\alpha$ -terpinene,  $\alpha$ -humulene, and  $\beta$ -caryophyllene, we could not identify any major intermediate products that are well-correlated with SOA growth (in both ozonolysis and photooxidation). It is possible that the first-generation products are not detected by the PTR-MS. In any case, we still observe a change in the rate of aerosol production for these compounds once the parent hydrocarbon is consumed. This suggests the occurrence of further reactions, as revealed by the continuously changing AMS delta time series after the complete consumption of the parent hydrocarbon – negative delta values continue to decrease while positive delta values continue to increase, suggesting the SOA is being further oxidized.

#### **2.5.2.7 $\beta$ -caryophyllene ozonolysis**

As noted above, there is a slight difference in the aerosol growth rate before and after the parent hydrocarbon is used up. This difference is very pronounced in the case of  $\beta$ -caryophyllene. Figure 2.17 shows the decay of the parent hydrocarbon and the corresponding aerosol growth. Due to the high reactivity of  $\beta$ -caryophyllene and ozone, a rapid decay of the parent hydrocarbon is observed; ~65% of the parent hydrocarbon is reacted in the first 25 minutes and the organic mass increases rapidly. When all  $\beta$ -caryophyllene is consumed at  $t = 50$  min, we observe a different slope in the rate of aerosol formation. This change in the rate of aerosol growth is likely due to the different mechanisms of aerosol formation. From  $t = 0$  min to  $t = 25$  min, the organic mass is most likely the nonvolatile first-generation products; from  $t = 25$  min to  $t = 50$  min, it is a mix of primary and secondary products; from  $t = 50$  min onwards, the reaction of first-

generation products with ozone becomes important, and so the aerosol growth results from the nonvolatile products that are formed from this further oxidation; Hoffmann et al. (17) observed evidence for aerosol growth from secondary products from this reaction as well. The amount of  $\beta$ -caryophyllene and ozone reacted over time is shown in Figure 2.18. The molar ratio of  $\beta$ -caryophyllene reacted to ozone consumed is almost 1:1 up to  $t = 25$  min, at which time  $\beta$ -caryophyllene is almost completely consumed, but ozone consumption continues to increase. The final amount of ozone consumed is approximately twice that of  $\beta$ -caryophyllene reacted, indicating that both double bonds are fully oxidized. The corresponding AMS delta series plot is shown in Figure 2.19. The fact that the negative delta values continue to decrease when all parent hydrocarbon is consumed indicates that the compounds are becoming increasingly oxidized.

#### **2.5.2.8 Longifolene photooxidation**

The growth curve from the photooxidation of longifolene, shown in Figure 2.20, appears to be anomalous. Aerosol mass increases as more longifolene is consumed; however, it appears that towards the end of the experiment aerosol growth stops even though the longifolene continues to be consumed. This atypical growth curve behavior is likely due to difficulties in obtaining good parent hydrocarbon and aerosol mass measurements. Products, or fragments of products, with the same mass to charge ratio as longifolene may be formed and interfere with the PTR-MS measurements. Another possibility is a change in the density of the aerosol over the course of the experiment, so that an accurate aerosol mass cannot be obtained from the DMA volumes and a fixed density. This is supported by our TDMA measurements, in which the increase in hygroscopic growth factor with RH is not monotonic (57) for longifolene photooxidation.

This could be indicative of large void volumes in the particles, potentially leading to large changes in the apparent density of the particles over the course of the experiment.

## **2.6 Implications for aerosol formation**

We report a series of chamber experiments investigating the formation of aerosols from the oxidation of a suite of biogenic hydrocarbons. Two main sets of experiments are performed: the ozonolysis of hydrocarbons in the dark and photooxidation experiments in which HONO is used as an OH precursor. Instead of the normal yield curve approach of plotting SOA yield as a function of the amount of aerosol formed, we present the data in terms of a growth curve, in which aerosol mass is plotted against the amount of hydrocarbon reacted over the course of the experiments. It is found that based on the shapes of these time-dependent growth curves, we can classify the compounds into two different groups based entirely on the number of double bonds of the parent hydrocarbon, regardless of their molecular formulas (isoprene, monoterpenes, sesquiterpenes or oxygenated terpenes). For compounds with only one double bond, aerosol mass increases as more hydrocarbon is consumed, and reaches a maximum when all the hydrocarbon is consumed, implying that the first oxidation step is rate-limiting and the aerosols are formed from nonvolatile first-generation products that partition into the aerosol phase once they are formed. For compounds with more than one double bond, aerosol mass continues to increase even after all hydrocarbon is consumed, resulting in a vertical section in the growth curve. This continuation in aerosol growth indicates the aerosol is formed from the further oxidation of first-generation products by ozone, and/or OH and NO<sub>3</sub> radicals in photooxidation experiments, and that this second oxidation step may also be rate-limiting. This work shows that the growth curve approach is a valuable means of

understanding the mechanisms of SOA formation by providing important information on the rate-determining steps and whether SOA is formed from first- or second-generation products.

Particularly revealing are the time-dependent growth curves for a number of experiments carried out over a range of initial hydrocarbon concentrations, and comparison of those curves with the final SOA growth curve allows us to examine whether it is appropriate to use time-dependent data to understand total SOA formation. It is found that for  $\alpha$ -pinene, the time-dependent growth curves describe the final growth data well, suggesting the parameters ( $\alpha_i$  and  $K_{om,i}$ ) can be determined from time-dependent data. This is likely the case for other compounds with only one double bond. Our observation implies that if the parent hydrocarbon has only one double bond, then instead of performing chamber experiments over a wide range of initial concentrations, one can simply carry out one experiment, and the time-dependent growth curve from that experiment will represent the final growth data. For terpinolene, the time-dependent growth curves and final SOA growth curve have dramatically different shapes. Therefore, for compounds with more than one double bond, the SOA is likely to have significant contributions from secondary products, and so one cannot simply use the time-dependent data to represent final growth data; instead we need to employ the standard approach, by carrying out experiments over a range of initial concentrations, until gas-phase oxidation is complete and gas-particle equilibrium is established. Thus, one has to be cautious when applying the SOA growth parameters ( $\alpha_i$  and  $K_{om,i}$ ) for systems with more than one double bond, making sure the data are obtained at final SOA growth conditions.

The experiments presented in this paper are performed at relatively high initial hydrocarbon concentrations; however, the same analysis should still be valid for lower SOA loadings, which are more atmospherically relevant. For the ozonolysis of both  $\alpha$ -pinene (compound with only one double bond) and terpinolene (compound with more than one double bond), we have shown that the time-dependent growth curves have the same general shape regardless of the initial hydrocarbon concentrations. Even with a  $M_o$  as low as  $20 \mu\text{g m}^{-3}$  such as in the ozonolysis of 12 ppb  $\alpha$ -pinene, the time-dependent growth curve still has the same shape as in the ozonolysis of 135 ppb  $\alpha$ -pinene. This suggests that the results described here should also apply to the atmospheric conditions in which organic aerosols loadings are smaller.

We have shown that for unsaturated biogenic hydrocarbons, the oxidative attack of each double bond determines the rate of SOA formation. Thus, in atmospheric models of SOA formation from compounds with more than one double bond, it is important that the first-generation products to be explicitly included. This requires the direct study of the chemistry of such intermediates, which presents a number of substantial experimental challenges. Donahue et al. (58) has recently developed a “basis-set” formalism to represent multiple oxidation stages in SOA formation; such an approach may be extremely useful for the inclusion of key intermediates, such as unsaturated oxidation products of biogenic hydrocarbons, in atmospheric models of SOA formation and growth.

## **2.7 Acknowledgements**

This research was funded by the U. S. Environmental Protection Agency Science to Achieve Results (STAR) Program grant number RD-83107501-0, managed by EPA's

Office of Research and Development (ORD), National Center for Environmental Research (NCER), and by U.S. Department of Energy Biological and Environmental Research Program DE-FG02-05ER63983. The University of California contribution to this material is based upon work supported by the National Science Foundation under Grant No. 0443448 and 0119510, and the California Air Resources Board (Contract 00-732). The authors would like to thank Neil M. Donahue for helpful discussions.

## 2.8 References

- (1) Turpin, B. J.; Huntzicker, J. J. Identifications of secondary organic aerosol episodes and quantification of primary and secondary organic aerosol concentration. *Atmos. Environ.* **1995**, *29*, 3527-3544.
- (2) Atkinson, R.; Arey, J. Gas-phase tropospheric chemistry of biogenic volatile organic compounds: a review. *Atmos. Environ.* **2003**, *37*, S197-S219.
- (3) Kanakidou, M. et al. Organic aerosol and global climate modelling: a review. *Atmos. Chem. Phys.*, **2005**, *5*, 1053-1123.
- (4) Hatakeyama, S; Izumi, K.; Fukuyama, T.; Akimoto, H. Reactions of ozone with  $\alpha$ -pinene and  $\beta$ -pinene in air: yields of gaseous and particulate products. *J. Geophys. Res.* **1989**, *94*, 13013-13024.
- (5) Christoffersen, T. S. et al. cis-pinic acid, a possible precursor for organic aerosol formation from ozonolysis of  $\alpha$ -pinene. *Atmos. Environ.* **1998**, *32*, 1657-1661.
- (6) Yu, J.; Flagan, R. C.; Seinfeld, J. H. Identification of products containing  $-\text{COOH}$ ,  $-\text{OH}$ , and  $-\text{C}=\text{O}$  in atmospheric oxidation of hydrocarbons. *Environ. Sci. Technol.* **1998**, *32*, 2357-2370.

- (7) Yu, J.; Cocker III, D. R.; Griffin, R. J.; Flagan, R. C.; Seinfeld, J. H. Gas-phase ozone oxidation of monoterpenes: gaseous and particulate products. *J. Atmos. Chem.* **1999**, *34*, 207-258.
- (8) Hoffmann, T.; Bandur, R.; Marggraf, U.; Linscheid, M. Molecular composition of organic aerosols formed in  $\alpha$ -pinene/O<sub>3</sub> reaction: implications for new particle formation process. *J. Geophys. Res.* **1998**, *103*, 25569-25578.
- (9) Griffin, R. J.; Cocker III, D.R.; Flagan, R. C.; Seinfeld, J. H. Organic aerosol formation from the oxidation of biogenic hydrocarbons. *J. Geophys. Res.* **1999**, *104*, 3555-3567.
- (10) Jang, M.; Kamens, R. M. Newly characterized products and composition of secondary aerosols from the reaction of  $\alpha$ -pinene with ozone. *Atmos. Environ.* **1999**, *33*, 459-474.
- (11) Glasius, M.; Lahaniati, M.; Calogirou, A.; Di Bella, D.; Jensen, N. R.; Hjorth, J.; Kotzias, D.; Larsen, B. R. Carboxylic acids in secondary aerosols from oxidation of cyclic monoterpenes by ozone. *Environ. Sci. Technol.* **2000**, *34*, 1001-1010.
- (12) Koch, S.; Winterhalter, R.; Uherek, E.; Kolloff, A.; Neeb, P.; Moortgat, G. K. Formation of new particles in the gas-phase ozonolysis of monoterpenes. *Atmos. Environ.* **2000**, *34*, 4031-4042.
- (13) Larsen, B. R.; Di Bella, D.; Glasius, M.; Winterhalter, R.; Jensen, N. R.; Hjorth, J. Gas-phase OH oxidation of monoterpenes: gaseous and particulate products. *J. Atmos. Chem.* **2001**, *38*, 231-276.

- (14) Kamens, R. M.; Jaoui, M. Modeling aerosol formation from  $\alpha$ -pinene+NO<sub>x</sub> in the presence of natural sunlight using gas-phase kinetics and gas-particle partitioning theory. *Environ. Sci. Technol.* **2001**, *35*, 1394-1405.
- (15) Jaoui, M.; Kamens, R. M. Mass balance of gaseous and particulate products analysis from  $\alpha$ -pinene/ NO<sub>x</sub>/air in the presence of natural sunlight. *J. Geophys. Res.* **2001**, *106*, 12541-12558.
- (16) Librando, V.; Tringali, G. Atmospheric fate of OH initiated oxidation of terpenes. Reaction mechanism of  $\alpha$ -pinene degradation and secondary organic aerosol formation. *J. Environ. Manage.* **2005**, *75*, 275-282.
- (17) Hoffmann, T.; Odum, J. R.; Bowman, F.; Collins, D.; Klockow, D.; Flagan, R. C.; Seinfeld, J. H. Formation of organic aerosols from the oxidation of biogenic hydrocarbons. *J. Atmos. Chem.* **1997**, *26*, 182-222.
- (18) Izumi, K.; Fukuyama, T. Photochemical aerosol formation from aromatic hydrocarbons in the presence of NO<sub>x</sub>. *Atmos. Environ.* **1990**, *24A*, 1433-1441.
- (19) Hurley, M. D.; Sokolov, O.; Wallington, T. J.; Takekawa, H.; Karasawa, M.; Klotz, B.; Barnes, I.; Becker, K. H. Organic aerosol formation during the atmospheric degradation of toluene. *Environ. Sci. Technol.* **2001**, *35*, 1358-1366.
- (20) Lee, A.; Goldstein, A.; Keywood, M. D.; Gao, S.; Ng, N. L.; Varutbangkul, V.; Bahreini, R.; Flagan, R. C.; Seinfeld, J. H. Gas-phase products and secondary aerosol yields from the ozonolysis of ten different terpenes. *J. Geophys. Res.* **2006**, in press.
- (21) Lee, A.; Goldstein, A.; Ng, N. L.; Kroll, J. H.; Varutbangkul, V.; Bahreini, R.; Flagan, R. C.; Seinfeld, J. H. Gas-phase products and secondary aerosol yields from the photooxidation of sixteen different terpenes. *J. Geophys. Res.* **2006**, submitted.



- (22) Presto, A. A.; Huff Hartz, K. E.; Donahue, N. M. Secondary organic aerosol production from terpene ozonolysis. 1. Effect of UV radiation. *Environ. Sci. Technol.* **2005**, *39*, 7036-7045.
- (23) Presto, A. A.; Huff Hartz, K. E.; Donahue, N. M. Secondary organic aerosol production from terpene ozonolysis. 2. Effect of NO<sub>x</sub> concentration. *Environ. Sci. Technol.* **2005**, *39*, 7046-7054.
- (24) Donahue, N. M.; Huff Hartz, K. E.; Chuong, B.; Preston, A. A.; Stanier, C. O.; Rosenhørn, T.; Robinson, A. L.; Pandis, S. N. Critical factors determining the variation in SOA yields from terpene ozonolysis: A combined experimental and computational study. *Faraday Discuss.* **2005**, *130*, 295-309.
- (25) Tolocka, M. P.; Jang, M.; Ginter, J. M.; Cox, F. J.; Kamens, R. M.; Johnston, M. V. Formation of oligomers in secondary organic aerosol. *Environ. Sci. Technol.* **2004**, *38*, 1428-1434.
- (26) Iinuma, Y.; Böge, O.; Gnauk, T.; Herrmann, H. Aerosol-chamber study of the  $\alpha$ -pinene/O<sub>3</sub> reaction: influence of particle acidity on aerosol yields and products. *Atmos Environ.* **2004**, *38*, 761-773.
- (27) Gao, S. et al. Particle phase acidity and oligomer formation in secondary organic aerosol. *Environ. Sci. Technol.* **2004**, *38*, 6582-6589.
- (28) Gao, S.; Keywood, M. D.; Ng, N. L.; Surratt, J. D.; Varutbangkul, V.; Bahreini, R.; Flagan, R.C.; Seinfeld, J.H. Low-molecular weight and oligomeric components in secondary organic aerosol from the ozonolysis of cycloalkenes and  $\alpha$ -pinene. *J. Phys. Chem. A*, **2004**, *108*, 10147-10164.

- (29) Kalberer, M.; Paulsen, D.; Sax, M.; Steinbacher, M.; Dommen, J.; Prevot, A. S. H.; Fisseha, R.; Weingartner, E.; Frankevich, V.; Zenobi, R.; Baltensperger, U. Identification of polymers as major components of atmospheric organic aerosols. *Science* **2004**, *303*, 1659-1662.
- (30) Odum J. R.; Hoffmann, T.; Bowman, F.; Collins, D.; Flagan, R. C.; Seinfeld, J. H. Gas/particle partitioning and secondary organic aerosol yields. *Environ. Sci. Technol.* **1996**, *30*, 2580-2585.
- (31) Pankow, J. F. An absorption-model of gas-particle partitioning of organic-compounds in the atmosphere. *Atmos. Environ.* **1994**, *28A*, 185-188.
- (32) Pankow, J. F. An absorption-model of the gas aerosol partitioning involved in the formation of secondary organic aerosol. *Atmos. Environ.* **1994**, *28A*, 189-193.
- (33) Odum, J. R.; Jungkamp, T. P. W.; Griffin, R. J.; Forstner, H. J. L.; Flagan, R. C.; Seinfeld, J. H. Aromatics, reformulated gasoline, and atmospheric organic aerosol formation. *Environ. Sci. Technol.* **1997**, *31*, 1890-1897.
- (34) Cocker III, D. R.; Clegg, S. L.; Flagan, R. C.; Seinfeld, J. H. The effect of water on gas-particle partitioning of secondary organic aerosol. Part 1:  $\alpha$ -pinene/ozone system. *Atmos. Environ.* **2001**, *35*, 6049-6072.
- (35) Cocker III, D. R.; Mader, B. T.; Kalberer, M.; Flagan, R. C.; Seinfeld, J. H. The effect of water on gas-particle partitioning of secondary organic aerosol. II: *m*-xylene and 1,3,5-trimethybenzene photooxidation systems. *Atmos. Environ.* **2001**, *35*, 6073-6085.
- (36) Keywood, M. D.; Varutbangkul, V.; Bahreini, R.; Flagan, R. C.; Seinfeld, J. H. Secondary organic aerosol formation from the ozonolysis of cycloalkenes and related compounds. *Environ. Sci. Technol.* **2004**, *38*, 4157-4164.

- (37) Chung, S. H.; Seinfeld, J. H. Global distribution and climate forcing of carbonaceous aerosols. *J. Geophys. Res.* **2002**, *107*, 4407, doi10.1029/2001JD001397.
- (38) Kroll, J. H.; Seinfeld, J. H. Representation of secondary organic aerosol (SOA) laboratory chamber data or the interpretation of mechanisms of particle growth. *Environ. Sci. Technol.* **2005**, *39*, 4159-4165.
- (39) Song, C.; Na, K.; Cocker III, D. R. Impact of the hydrocarbon to NO<sub>x</sub> ratio on secondary organic aerosol formation. *Environ. Sci. Technol.* **2005**, *39*, 3143-3149.
- (40) Holzinger, R.; Lee, A.; Paw U, K. T.; Goldstein, A. H. Observation of oxidation products above a forest imply biogenic emissions of very reactive compounds. *Atmos. Chem. Phys.* **2005**, *5*, 67-75.
- (41) Cocker III, D. R.; Flagan, R. C.; Seinfeld, J. H. State-of-the-art chamber facility for studying atmospheric aerosol chemistry. *Environ. Sci. Technol.* **2001**, *35*, 2594-2601.
- (42) Lindinger, W.; Hansel, A.; Jordan, A. Proton-transfer-reaction mass spectrometry (PTR-MS): on-line monitoring of volatile organic compounds at pptv levels. *Chem. Soc. Rev.* **1998**, *27*, 347-354.
- (43) Jayne, J. T.; Leard, D. C.; Zhang, X.; Davidovits, P.; Smith, K. A.; Kolb, C. E.; Worsnop, D. W. Development of an Aerosol Mass Spectrometer for size and composition analysis of submicron particles. *Aerosol Sci. and Technol.* **2000**, *33*, 49-70.
- (44) Allan, J. D.; Jimenez, J. L.; Coe, H.; Bower, K. N.; Williams, P. I.; Worsnop, D. R. Quantitative sampling using an Aerodyne Aerosol Mass Spectrometer. Part 1: Techniques of data interpretation and error analysis. *J. Geophys. Res.* **2003**, *108*, 4090, doi:4010.1029/2002JD002358.

- (45) Allan, J. D.; Bower, K. N.; Coe, H.; Boudries, H.; Jayne, J. T.; Canagaratna, M. R.; Millet, D. B.; Goldstein, A. H.; Quinn, P. K.; Weber, R. J.; Worsnop, D. R. Submicron aerosol composition at Trinidad Head, California, during ITCT 2K2: Its relationship with gas phase volatile organic carbon and assessment of instrument performance. *J. Geophys. Res.*, **2004**, *109*, D23S24, doi:10.1029/2003JD004208.
- (46) Bahreini, R.; Keywood, M. D.; Ng, N. L.; Varutbangkul, V.; Gao, S.; Flagan, R. C.; Seinfeld, J. H. Measurements of secondary organic aerosol (SOA) from oxidation of cycloalkenes, terpenes, and *m*-xylene using an Aerodyne aerosol mass spectrometer. *Environ. Sci. Technol.* **2005**, *39*, 5674-5688.
- (47) McLafferty, F. W.; Turecek, F. *Interpretation of Mass Spectra*; University Science Books; Sausalito, 1993.
- (48) Kamens, R. M.; Jang, M.; Chien, C. J.; Leach, K. Aerosol formation from the reaction of  $\alpha$ -pinene and ozone using a gas-phase kinetics-aerosol partition model. *Environ. Sci. Technol.* **1999**, *33*, 1430-1438.
- (49) Jenkin, M. E.; Shallcross, D. E.; Harvey, J. N. Development and application of a possible mechanism for the generation of cis-pinic acid from the ozonolysis of  $\alpha$ - and  $\beta$ -pinene. *Atmos. Environ.* **2000**, *34*, 2837-2850.
- (50) Hallquist, M.; Wängberg, I.; Ljungström, E. Atmospheric fate of carbonyl oxidation products originating from  $\alpha$ -pinene and  $\Delta^3$ -carene: determination of rate of reaction with OH and NO<sub>3</sub> radicals, UV absorption cross sections, and vapor pressures. *Environ. Sci. Technol.* **1997**, *31*, 3166-3172.

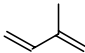
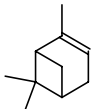
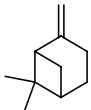
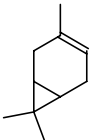
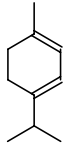
- (51) Hatakeyama, S; Izumi, K.; Fukuyama, T.; Akimoto, H.; Washida, N. Reactions of OH with  $\alpha$ -pinene and  $\beta$ -pinene in air: estimate of global CO production from the atmospheric oxidation of terpenes. *J. Geophys. Res.* **1991**, *96*, 947-958.
- (52) Hakola, H.; Arey, J.; Aschmann, S. M.; Atkinson, R. Product formation from the gas-phase reactions of OH radicals and O<sub>3</sub> with a series of monoterpenes. *J. Atmos. Chem.* **1994**, *18*, 75-102.
- (53) Reissell, A.; Harry, C.; Aschmann, S. M.; Atkinson, R.; Arey, J. Formation of acetone from the OH radical- and O<sub>3</sub>-initiated reactions of a series of monoterpenes. *J. Geophys. Res.* **1999**, *104*, 13869-13879.
- (54) Kwok, E. S. C.; Atkinson, R. Estimation of hydroxyl radical reaction rate constants for gas-phase organic compounds using a structure-reactivity relationship: an update. *Atmos. Environ.* **1995**, *29*, 1685-1695.
- (55) Kroll, J. H.; Ng, N. L.; Murphy, S. M.; Flagan, R. C.; Seinfeld, J. H. Secondary organic aerosol formation from isoprene photooxidation under high-NO<sub>x</sub> conditions. *Geophys. Res. Lett.* 2005, *32*, L18808, doi:10.1029/2005GL023637.
- (56) Kroll, J. H.; Ng, N. L.; Murphy, S. M.; Flagan, R. C.; Seinfeld, J. H. Secondary organic aerosol formation from isoprene photooxidation. *Environ. Sci. Technol.* **2006**, in press.
- (57) Varutbangkul, V. et al. Hygroscopicity of secondary organic aerosols formed by oxidation of cycloalkenes, monoterpenes, sesquiterpenes and related compounds, *Atmos. Chem. Phys.* **2006**, submitted.

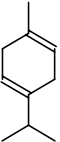
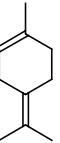
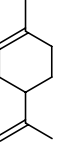
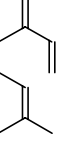
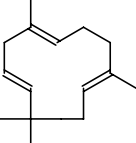
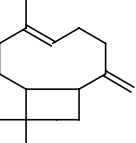
(58) Donahue, N. M.; Robinson, A. L.; Stanier, C. O.; Pandis, S. N. The coupled partitioning, dilution, and chemical aging of semivolatile organics. *Environ. Sci. Technol.* **2006**, in press.

(59) Reissell, A.; Aschmann, S. M.; Atkinson, R.; Arey, J. Products of the OH radical- and O<sub>3</sub>-initiated reactions of myrcene and ocimene. *J. Geophys. Res.* **2002**, *107*, 4138, doi:10.1029/2001JD001234.

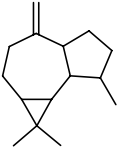
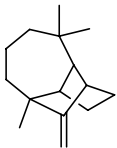
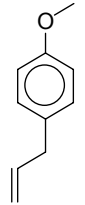
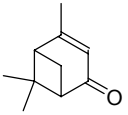
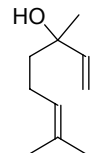
(60) Shu, Y.; Kwok, E. S. C.; Tuazon, E. C.; Atkinson, R.; Arey, J. Products and gas-phase reactions of linalool with OH radicals, NO<sub>3</sub> radicals, and O<sub>3</sub>. *Environ. Sci. Technol.* **1997**, *31*, 896-904.

Table 2. 1. Parent hydrocarbon studied

Parent Hydrocarbon	Structure	Formula (MW)	$k_{\text{Ozone}} (\text{cm}^3 \text{ molec}^{-1} \text{ s}^{-1})^a$	$k_{\text{OH}} (\text{cm}^3 \text{ molec}^{-1} \text{ s}^{-1})^a$
isoprene		$\text{C}_5\text{H}_8$ (68)	NS	$9.9 \times 10^{-11}$
$\alpha$ -pinene		$\text{C}_{10}\text{H}_{16}$ (136)	$8.4 \times 10^{-17}$	$5.3 \times 10^{-11}$
$\beta$ -pinene		$\text{C}_{10}\text{H}_{16}$ (136)	$1.5 \times 10^{-17}$	$7.7 \times 10^{-11}$
$\Delta^3$ -carene		$\text{C}_{10}\text{H}_{16}$ (136)	$3.7 \times 10^{-17}$	$8.7 \times 10^{-11}$
$\alpha$ -terpinene		$\text{C}_{10}\text{H}_{16}$ (136)	$2.1 \times 10^{-14}$	$3.6 \times 10^{-10}$

$\gamma$ -terpinene		$C_{10}H_{16}$ (136)	NS	$1.8 \times 10^{-10}$
terpinolene		$C_{10}H_{16}$ (136)	$1.9 \times 10^{-15}$	$2.3 \times 10^{-10}$
limonene		$C_{10}H_{16}$ (136)	NS	$1.7 \times 10^{-10}$
myrcene		$C_{10}H_{16}$ (136)	$4.7 \times 10^{-16}$	$2.1 \times 10^{-10}$
$\alpha$ -humulene		$C_{15}H_{24}$ (204)	$1.17 \times 10^{-14}$	$3.0 \times 10^{-10}$
$\beta$ -caryophyllene		$C_{15}H_{24}$ (204)	$1.16 \times 10^{-14}$	$2.0 \times 10^{-10}$



aromadendrene		$C_{15}H_{24}$ (204)	NS	N/A
longifolene		$C_{15}H_{24}$ (204)	NS	$4.8 \times 10^{-11}$
methyl chavicol		$C_{10}H_{12}O$ (148)	$1.7 \times 10^{-17}{}^b$	N/A
verbenone		$C_{10}H_{14}O$ (150)	NS	N/A
linalool		$C_{10}H_{18}O$ (154)	$6 \times 10^{-16}{}^b$	$1.6 \times 10^{-10}$

a: Rate constants obtained from Atkinson and Arey (2) and references therein

b: Rate constants estimated from the rate of hydrocarbon decay

NS: Compounds not studied in ozonolysis experiments; N/A: Data not available

Table 2. 2. Initial conditions and data for ozonolysis experiments

Date	Parent Hydrocarbon	T (K)	RH (%)	Seed	$\Delta\text{HC}$ (ppb)	$\Delta\text{M}_o$ ( $\mu\text{g}/\text{m}^3$ )
3/24/2003	$\alpha$ -pinene	292	4.1	(NH <sub>4</sub> ) <sub>2</sub> SO <sub>4</sub>	186	419
3/12/2003	$\beta$ -pinene	293	6.3	(NH <sub>4</sub> ) <sub>2</sub> SO <sub>4</sub>	180	174
4/4/2003	$\Delta^3$ -carene	293	6.5	(NH <sub>4</sub> ) <sub>2</sub> SO <sub>4</sub>	90	273
3/31/2003	$\alpha$ -terpinene	293	3.4	(NH <sub>4</sub> ) <sub>2</sub> SO <sub>4</sub>	61	160
3/31/2003	terpinolene	293	5.5	(NH <sub>4</sub> ) <sub>2</sub> SO <sub>4</sub>	112	124
4/2/2003	myrcene	293	6.7	(NH <sub>4</sub> ) <sub>2</sub> SO <sub>4</sub>	98	61
3/28/2003	$\alpha$ -humulene	293	4.5	None	111	416
3/21/2003	$\beta$ -caryophyllene	293	6.2	None	88	336
4/4/2003	methyl chavicol	292	4.0	(NH <sub>4</sub> ) <sub>2</sub> SO <sub>4</sub>	101	40
4/2/2003	linalool	292	4.0	(NH <sub>4</sub> ) <sub>2</sub> SO <sub>4</sub>	106	8

Table 2. 3. Initial conditions and data for photooxidation experiments

Date	Parent Hydrocarbon	T (K)	RH (%)	Seed	$\Delta\text{HC}$ (ppb)	$\Delta\text{M}_0$ ( $\mu\text{g}/\text{m}^3$ )	$\frac{\text{ppbHC}}{\text{ppbNO}_x}$
3/4/2005	isoprene	294	54	(NH <sub>4</sub> ) <sub>2</sub> SO <sub>4</sub>	506	26	1.8
3/9/2005	$\alpha$ -pinene	293	43	(NH <sub>4</sub> ) <sub>2</sub> SO <sub>4</sub>	108	198	1.1
3/9/2005	$\beta$ -pinene	293	50	(NH <sub>4</sub> ) <sub>2</sub> SO <sub>4</sub>	170	293	2.1
3/12/2005	$\Delta^3$ -carene	294	52	(NH <sub>4</sub> ) <sub>2</sub> SO <sub>4</sub>	109	236	0.8
3/24/2005	$\alpha$ -terpinene	293	47	(NH <sub>4</sub> ) <sub>2</sub> SO <sub>4</sub>	103	145	0.9
3/21/2005	$\gamma$ -terpinene	294	48	(NH <sub>4</sub> ) <sub>2</sub> SO <sub>4</sub>	119	193	1.1
3/23/2005	terpinolene	294	50	(NH <sub>4</sub> ) <sub>2</sub> SO <sub>4</sub>	110	190	1.1
3/25/2005	limonene	294	45	(NH <sub>4</sub> ) <sub>2</sub> SO <sub>4</sub>	120	394	1.1
3/22/2005	myrcene	294	53	(NH <sub>4</sub> ) <sub>2</sub> SO <sub>4</sub>	112	272	0.9
3/16/2005	$\alpha$ -humulene	294	53	None	46	254	1.4
3/14/2005	$\beta$ -caryophyllene	295	56	None	37	212	1.3
3/15/2005	aromadendrene	294	47	None	34	107	1.4
3/19/2005	longifolene	294	49	None	34	186	0.8
3/26/2005	methyl chavicol	294	49	(NH <sub>4</sub> ) <sub>2</sub> SO <sub>4</sub>	79	194	0.8
3/31/2005	verbenone	294	46	(NH <sub>4</sub> ) <sub>2</sub> SO <sub>4</sub>	105	127	1.1
4/1/2005	linalool	295	40	(NH <sub>4</sub> ) <sub>2</sub> SO <sub>4</sub>	124	104	1.0

Table 2. 4. Ozonolysis - major first-generation products and their molar yields

<b>Date</b>	<b>Parent Hydrocarbon (more than one double bond)</b>	<b>m/z of major first-generation products</b>	<b>Product Molar Yield</b>
3/31/2003	$\alpha$ -terpinene	N/A	N/A
3/31/2003	terpinolene	111 (4-methyl-3-cyclohexen-1-one ) <sup>a</sup>	0.58 <sup>b</sup>
4/2/2003	myrcene	111 (4-vinyl-4-pentenal) <sup>c</sup>	0.53 <sup>b</sup>
3/28/2003	$\alpha$ -humulene	N/A	N/A
3/21/2003	$\beta$ -caryophyllene	N/A	N/A

N/A: No major first-generation products are observed to correlate with aerosol growth

a: Previously identified by Hakola et al. (52) and Reissell et al. (53)

b: Sum of yields of m/z 111 and m/z 93, the dehydrated fragment of m/z 111

c: Previously identified by Reissell et al. (59)

Table 2. 5. Photooxidation - major first-generation products and their molar yields

Date	Parent Hydrocarbon (more than one double bond)	m/z of major first-generation products	Product Molar Yield
3/4/2005	isoprene	71 (methacrolein + MVK)	0.79
3/24/2005	$\alpha$ -terpinene	N/A	N/A
3/21/2005	$\gamma$ -terpinene	153	0.05
		169 ( $\gamma$ -terpinaldehyde)	0.58 <sup>a</sup>
3/23/2005	terpinolene	111 (4-methyl-3-cyclohexen-1-one) <sup>b</sup>	0.47 <sup>c</sup>
3/25/2005	limonene	169 (limononaldehyde) <sup>d</sup>	0.61 <sup>e</sup>
3/22/2005	myrcene	93	0.34
		113	0.36
3/16/2005	$\alpha$ -humulene	N/A	N/A
3/14/2005	$\beta$ -caryophyllene	N/A	N/A
4/1/2005	linalool	129 (4-hydroxy-4-methyl-5-hexen-1-al) <sup>f</sup>	0.74 <sup>g</sup>

N/A: No major first-generation products are observed to correlate with aerosol growth

a: Sum of yields of all fragments and isotopes of m/z 169 (i.e. m/z 107, m/z 123, m/z 124, m/z 151, m/z 152 and m/z 170)

b: Previously identified by Hakola et al. (52) and Reissell et al. (53)

c: Sum of yields of m/z 111 and m/z 93, the dehydrated fragment of m/z 111

d: Previously identified by Hakola et al. (52)

e: Sum of yields of all fragments and isotopes of m/z 169 (i.e. m/z 107, m/z 108, m/z 123, m/z 124, m/z 133, m/z 151, m/z 152 and m/z 170)

f: Previously identified by Shu et al. (60)

g: Sum of yields of m/z 129, m/z 111 and m/z 93, the dehydrated fragments of m/z 129

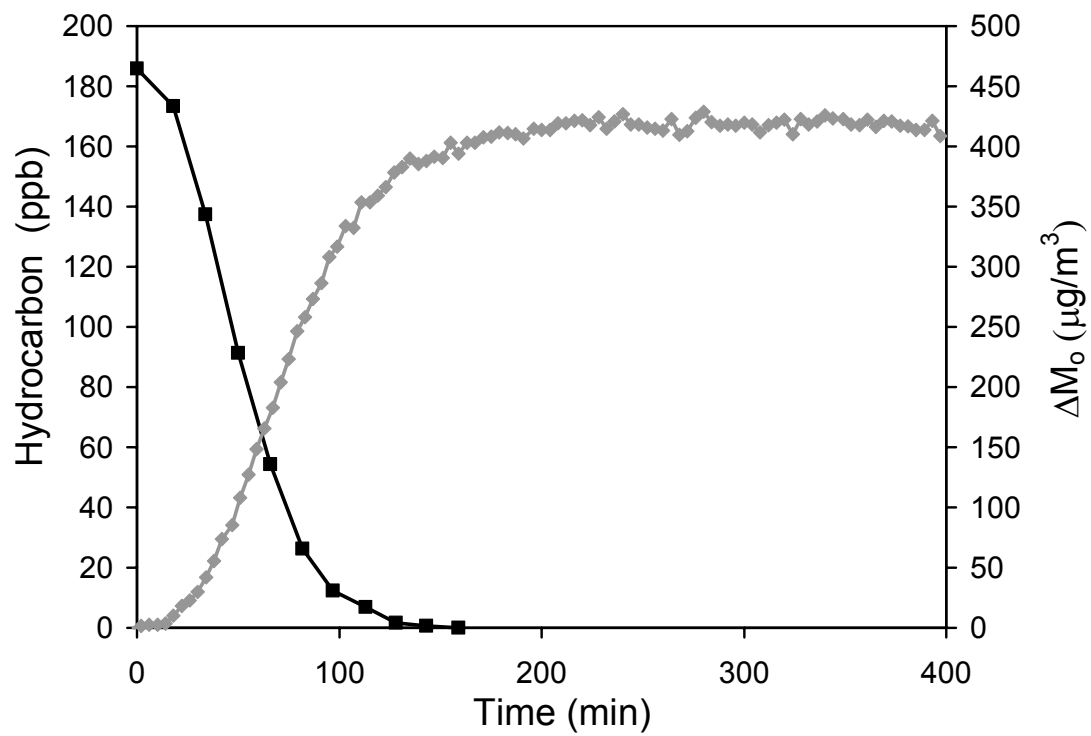
Figure 2. 1.  $\alpha$ -pinene ozonolysis and aerosol mass formation

Figure 2. 2. Terpinolene ozonolysis and aerosol mass formation

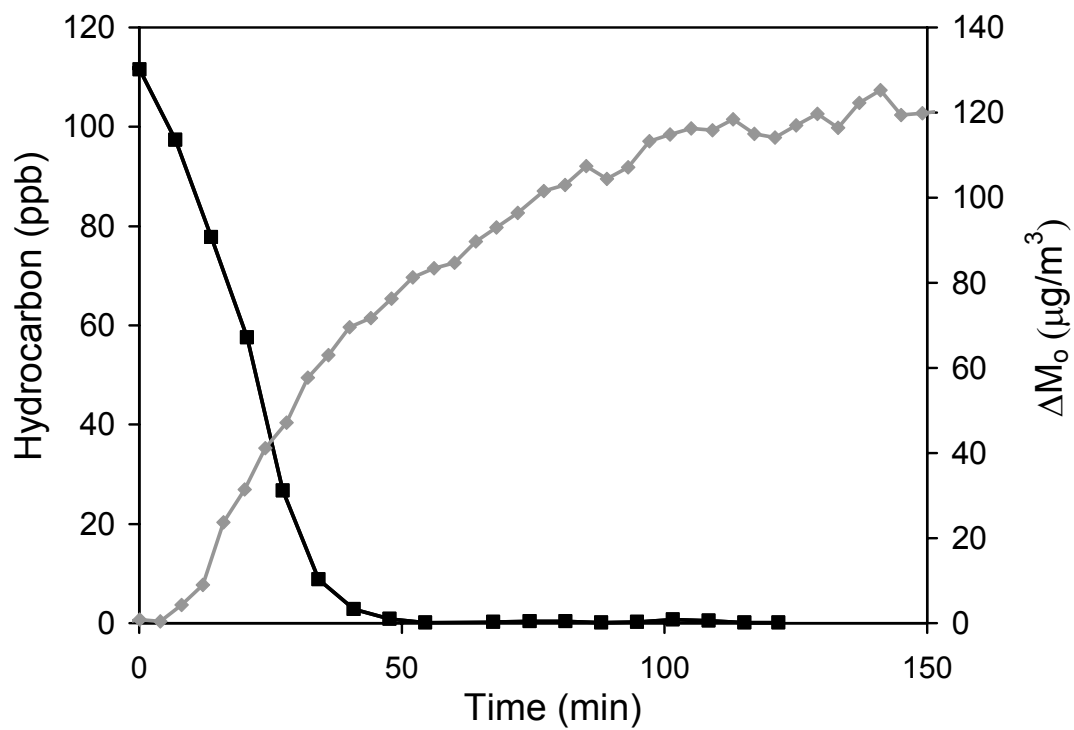


Figure 2. 3. Time-dependent growth curves for all compounds studied in ozonolysis experiments (except linalool, which does not have significant aerosol growth), note that the axes have different scales.

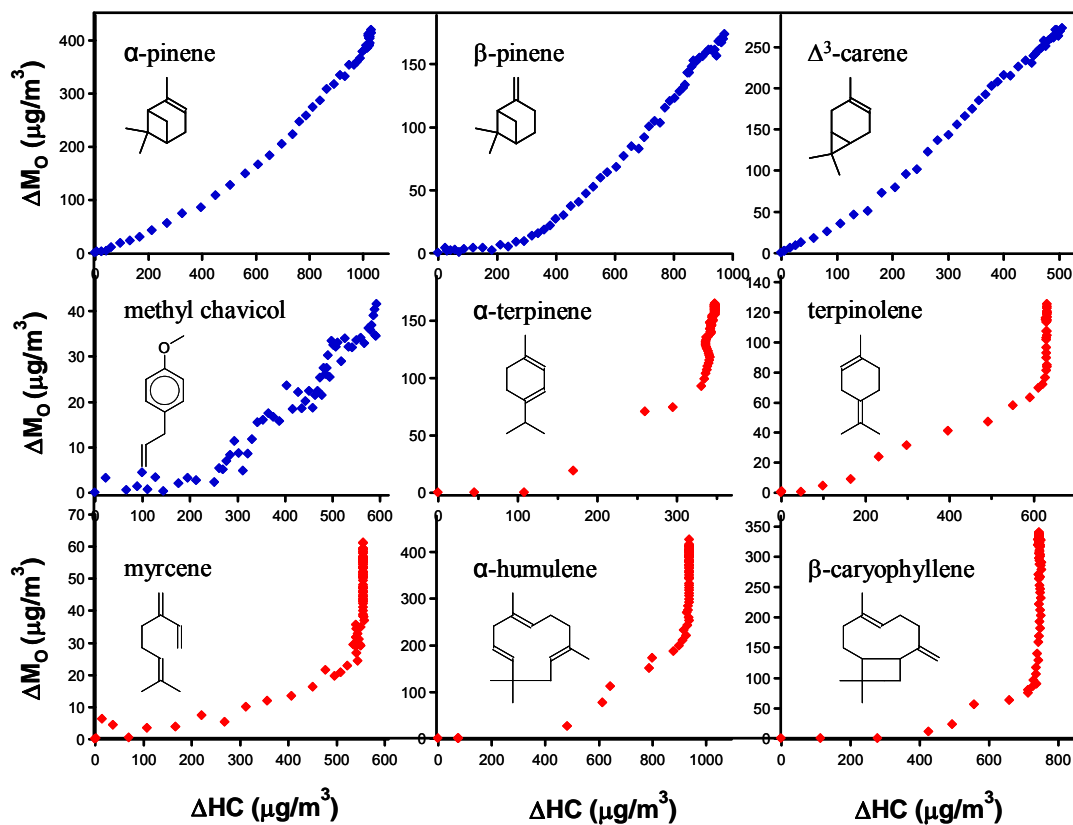




Figure 2. 4. Time-dependent growth curves for all compounds studied in photooxidation experiments (except longifolene, which is shown in Figure 2.20), note that the axes have different scales.

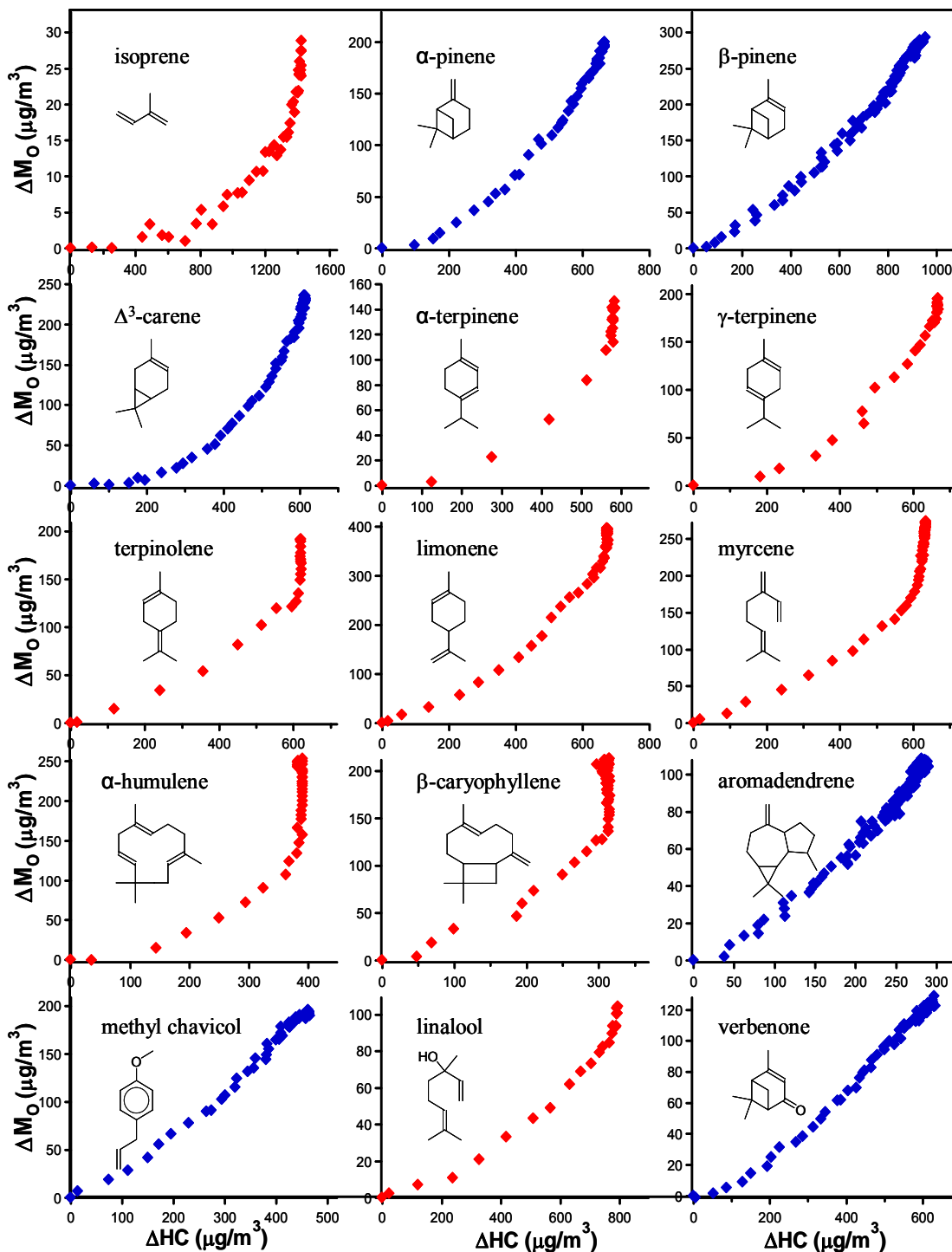


Figure 2. 5. Time-dependent and final growth curves for  $\alpha$ -pinene ozonolysis. The large diamonds represent final growth data through which the yield curve has been fit.

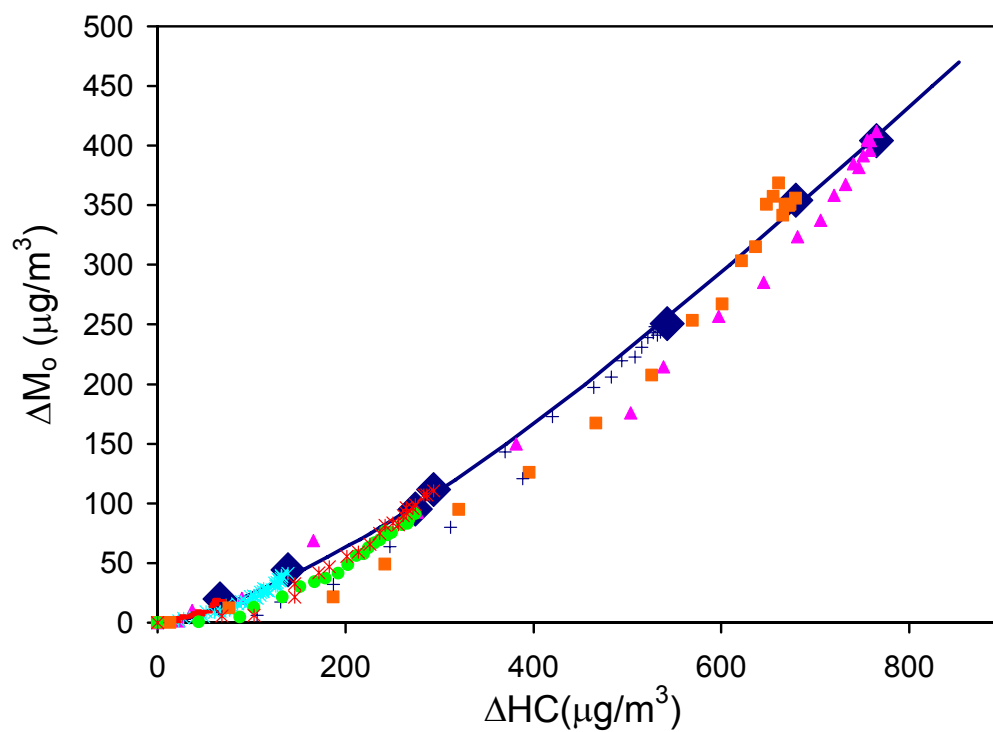


Figure 2. 6. AMS relative delta time series plot for  $\alpha$ -pinene ozonolysis. Unsaturated organics yield delta values  $\leq 0$ , and oxygenated organics yield delta values  $\geq 2$ .

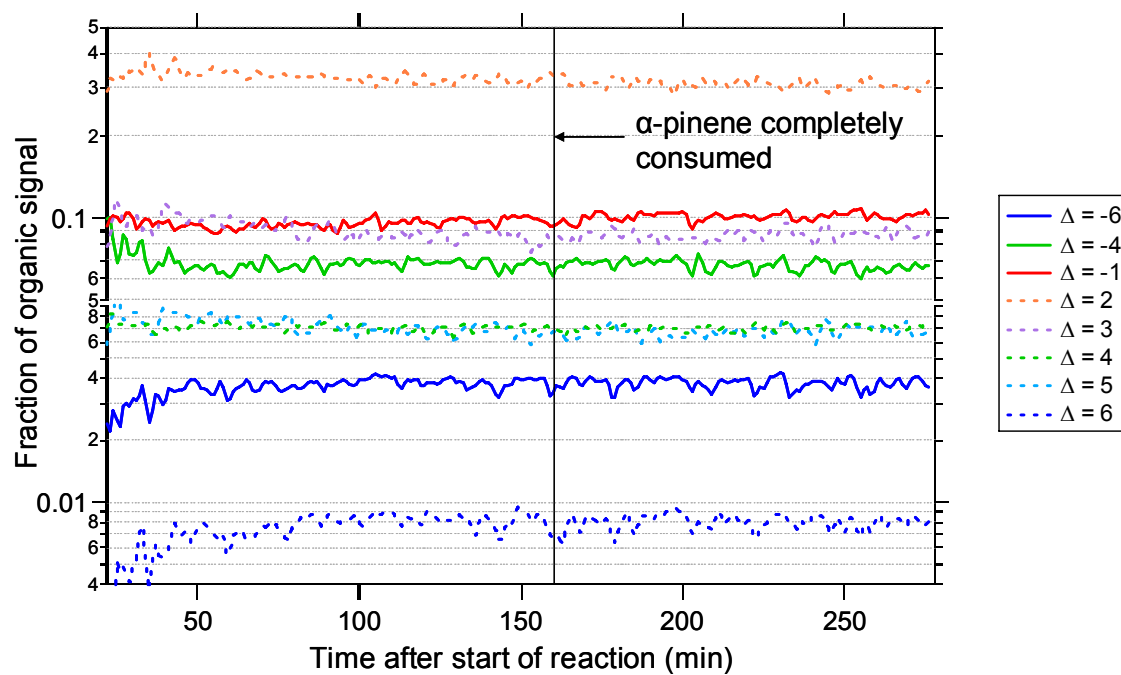


Figure 2. 7. Time-dependent and final growth curves for terpinolene ozonolysis. The large diamonds represent final growth data through which the yield curve has been fit.

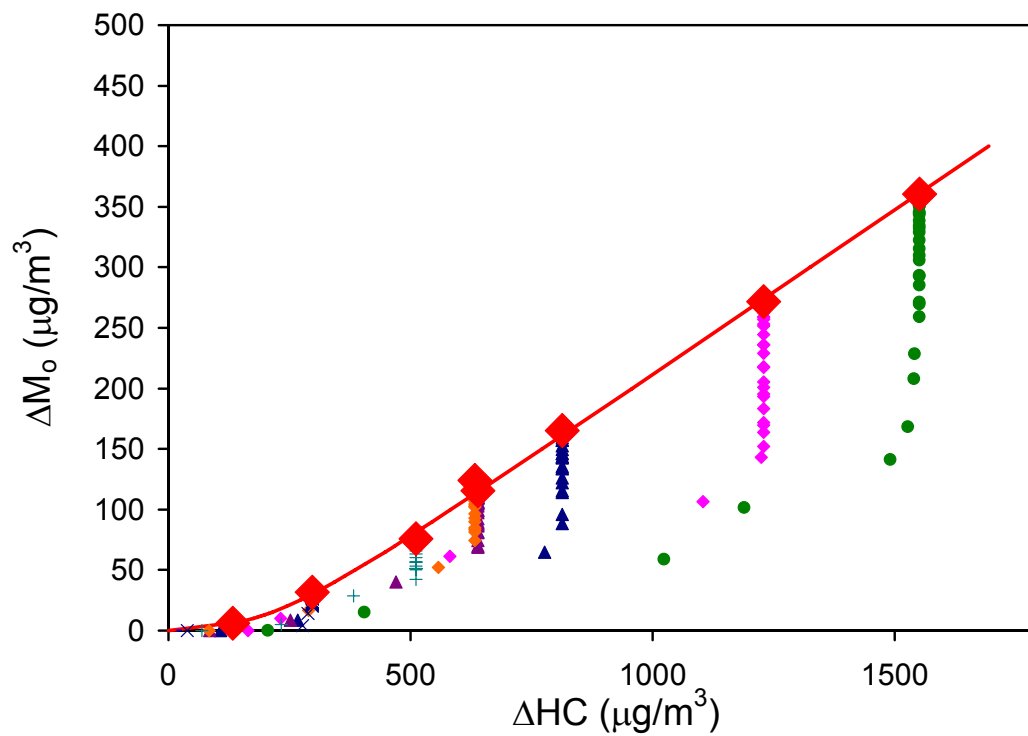


Figure 2. 8. Time evolution of pinonaldehyde in  $\alpha$ -pinene ozonolysis. The concentration of pinonaldehyde is the average of the upper and lower limits measured by PTR-MS (20).

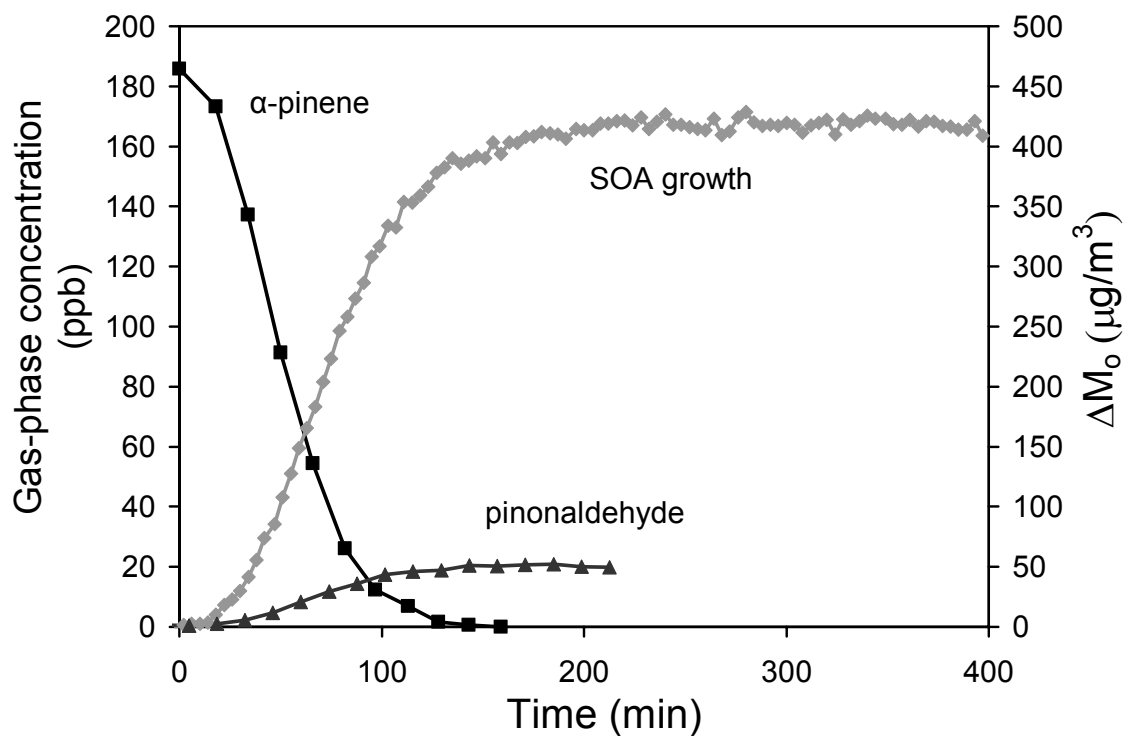


Figure 2. 9. Time evolution of pinonaldehyde in  $\alpha$ -pinene photooxidation. The concentration of pinonaldehyde is the mid-range mixing ratio measured by PTR-MS (21).

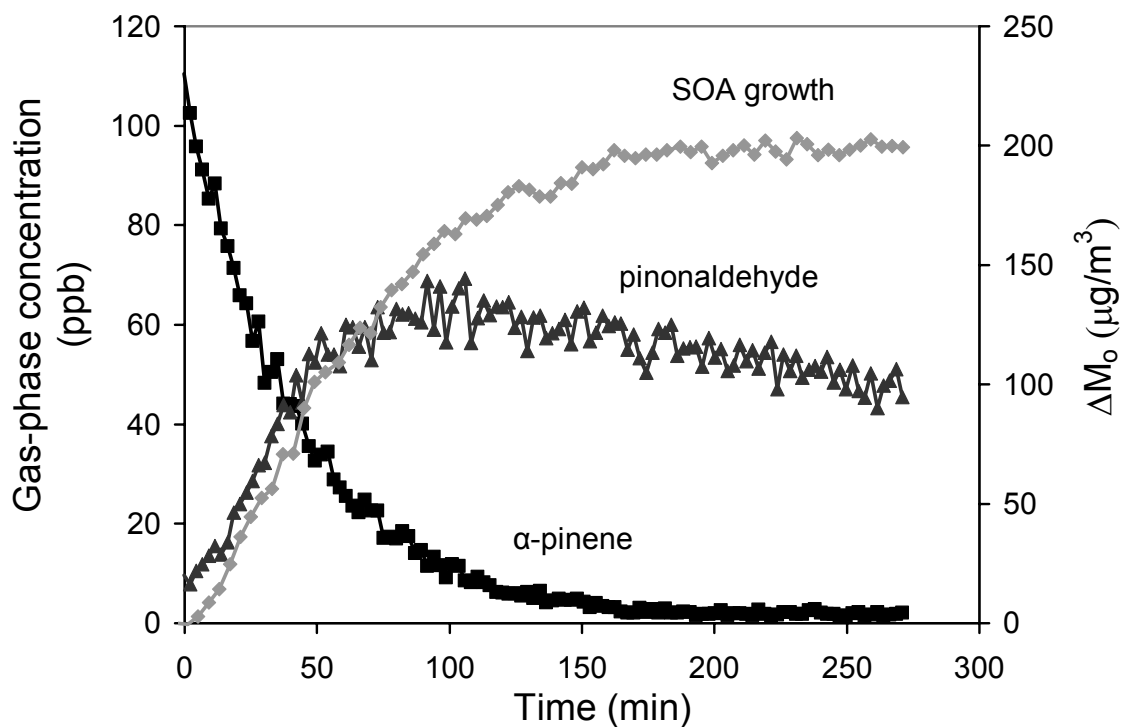


Figure 2. 10. Time evolution of m/z 93 and m/z 111 ions for terpinolene ozonolysis; m/z 93 is the dehydrated fragment of m/z 111.

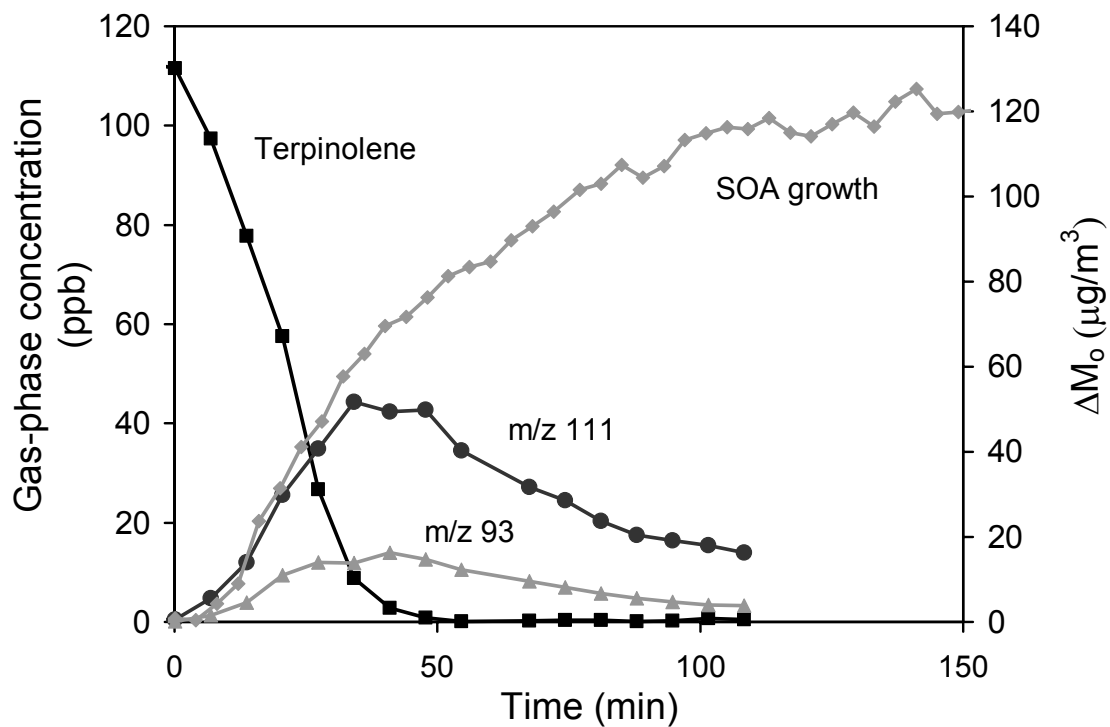


Figure 2. 11. The amount of the intermediate product  $m/z$  111 (including the dehydrated fragment  $m/z$  93) measured, formed and reacted over time for terpinolene ozonolysis

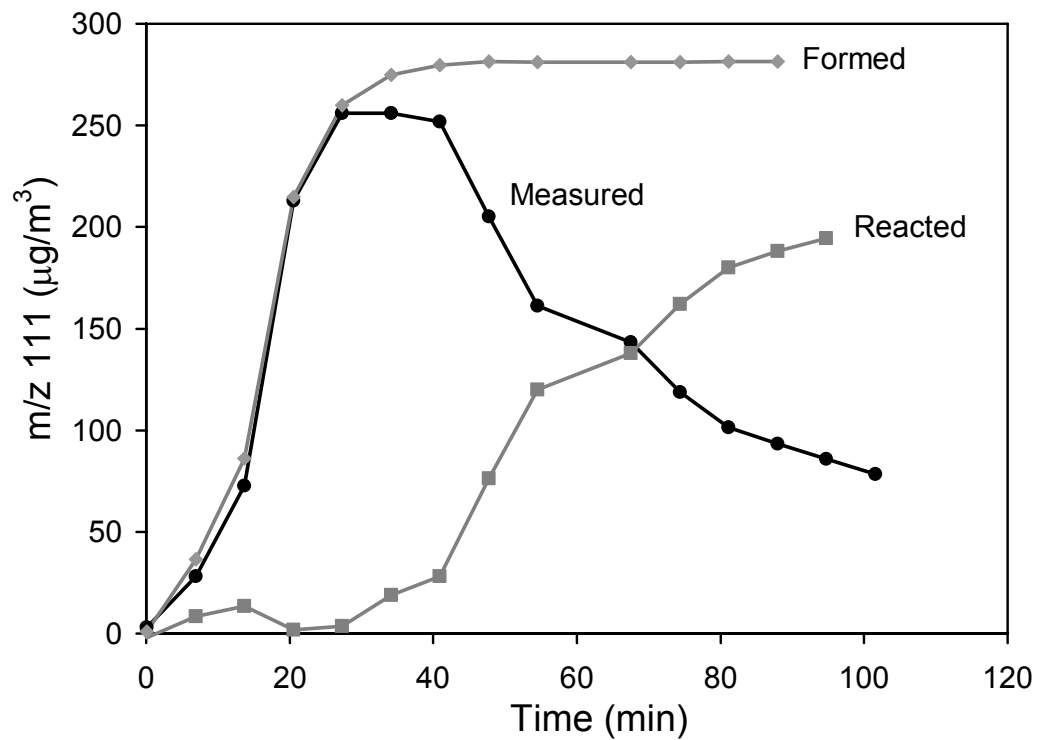




Figure 2. 12. SOA mass formed as a function of the amount of the intermediate product  $m/z$  111 reacted for terpinolene ozonolysis

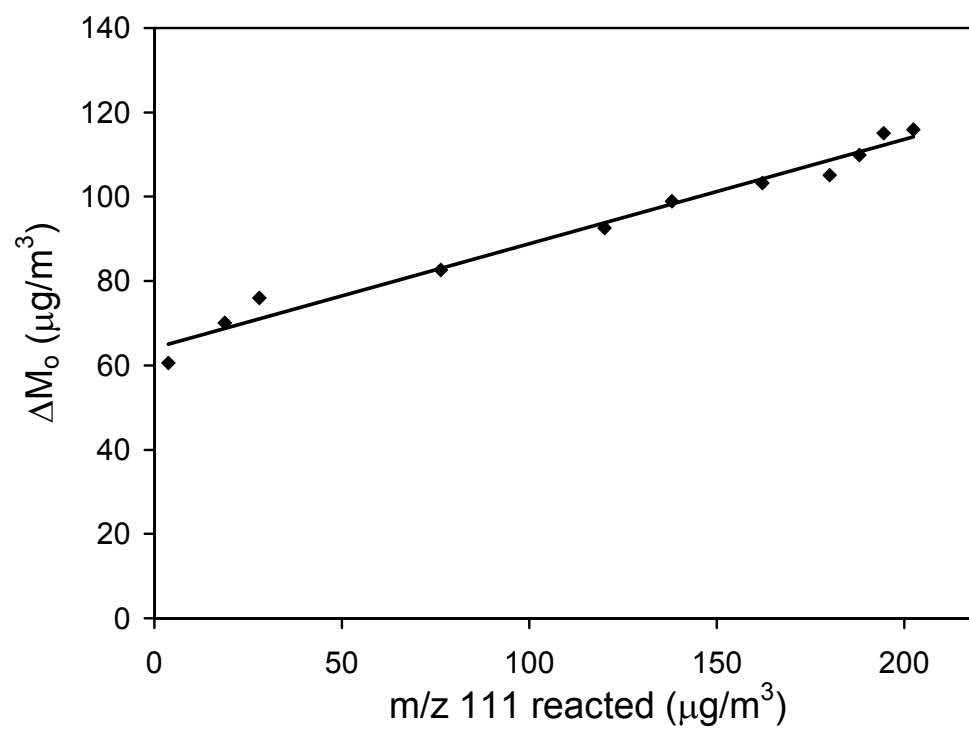


Figure 2. 13. SOA mass formed as a function of the amount of the intermediate product  $m/z$  111 reacted for terpinolene photooxidation

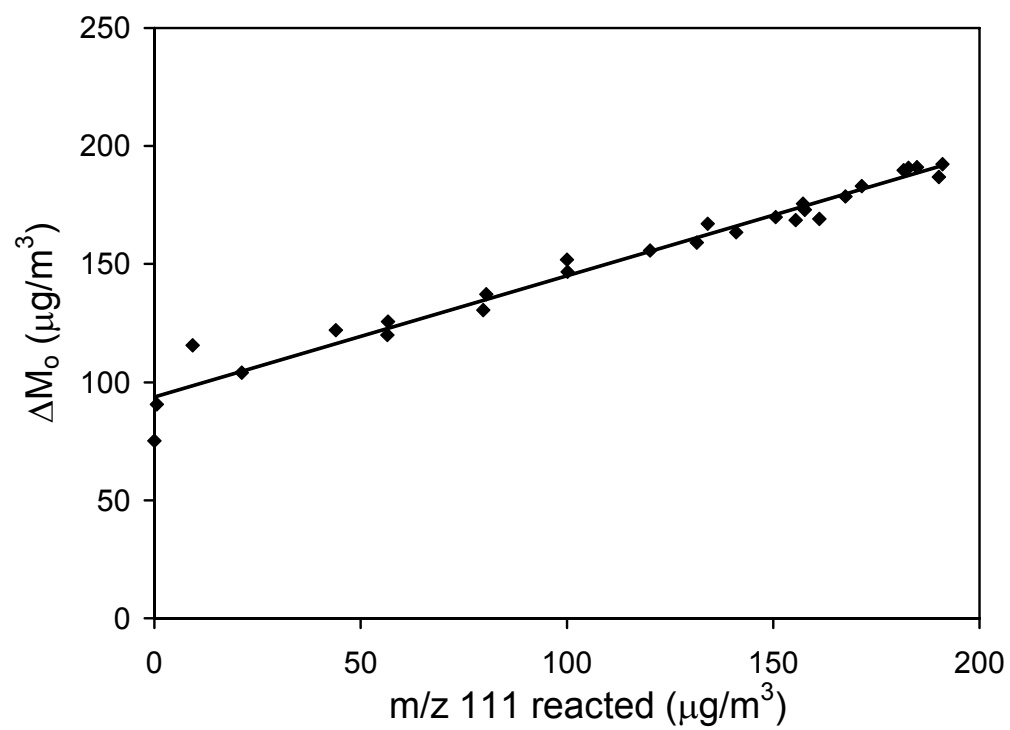


Figure 2. 14. SOA mass formed as a function of the amount of the intermediate product  $m/z$  169 (including its fragments and isotopes) reacted for limonene photooxidation

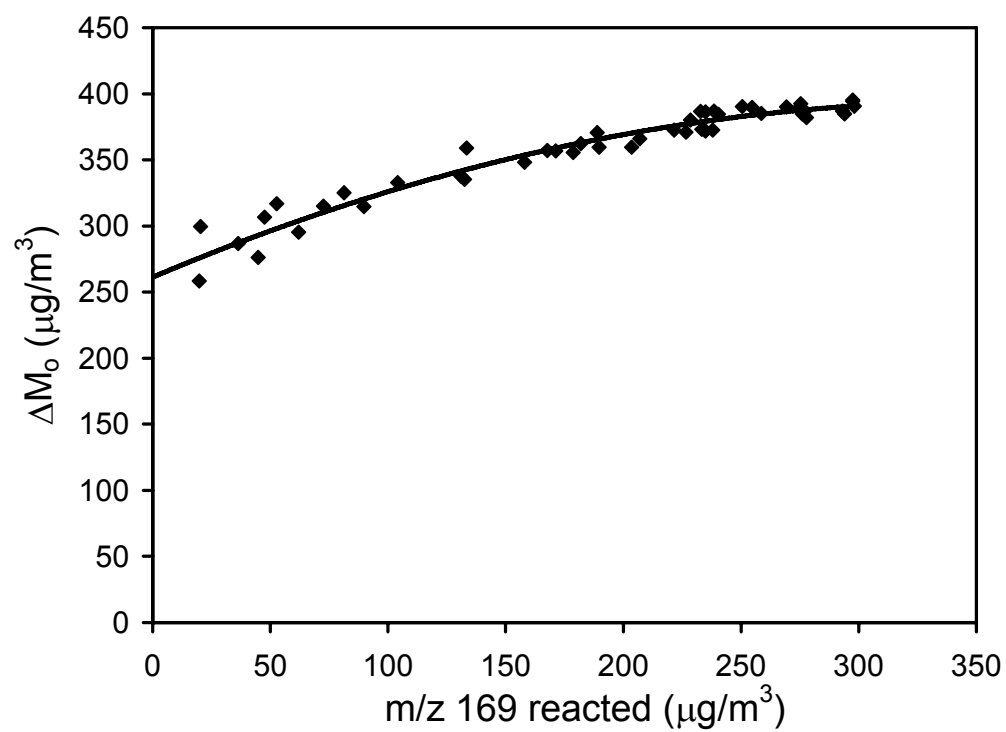


Figure 2. 15. Time evolution of methacrolein + methyl vinyl ketone for isoprene photooxidation

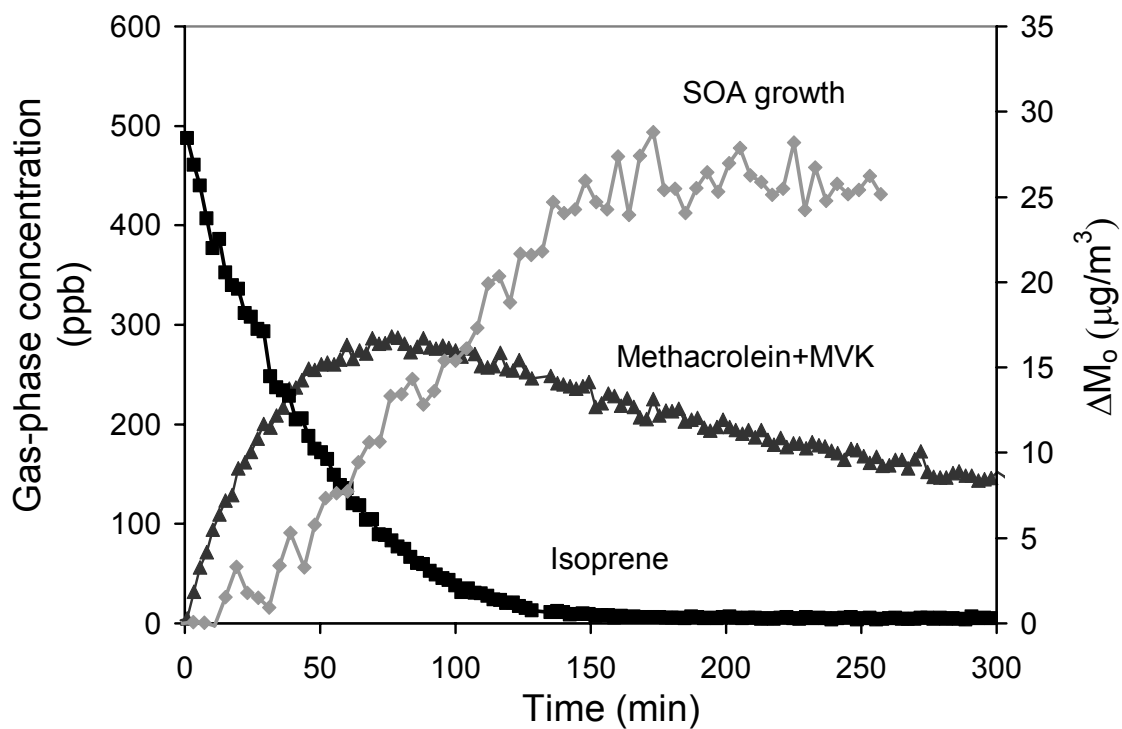


Figure 2. 16. SOA mass formed as a function of the amount of the methacrolein + methyl vinyl ketone reacted for isoprene photooxidation

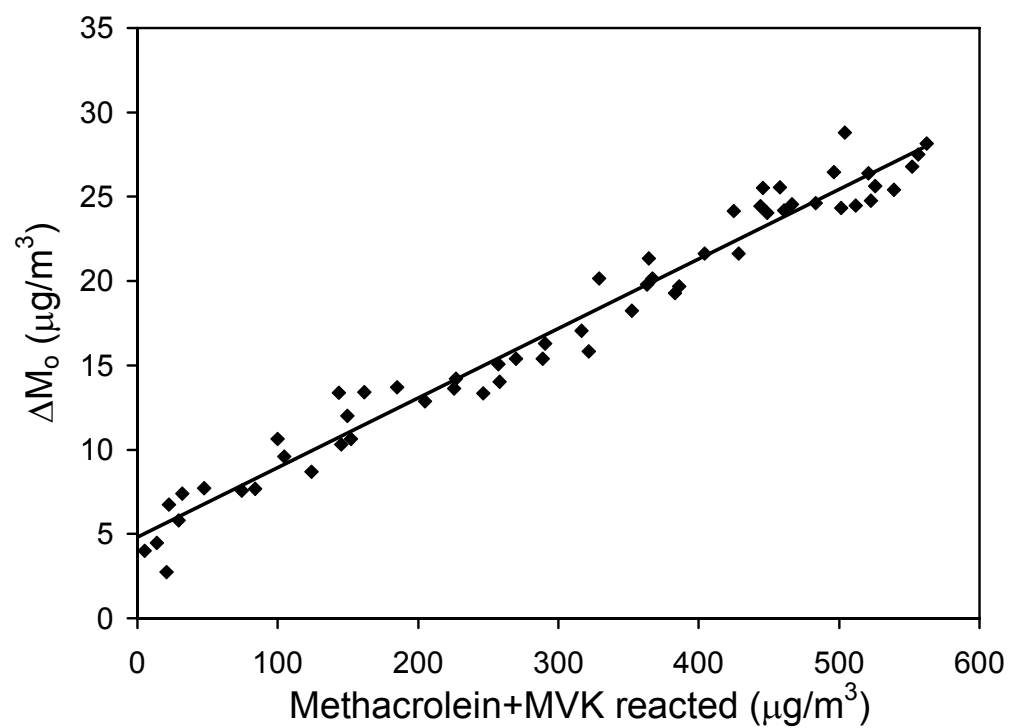


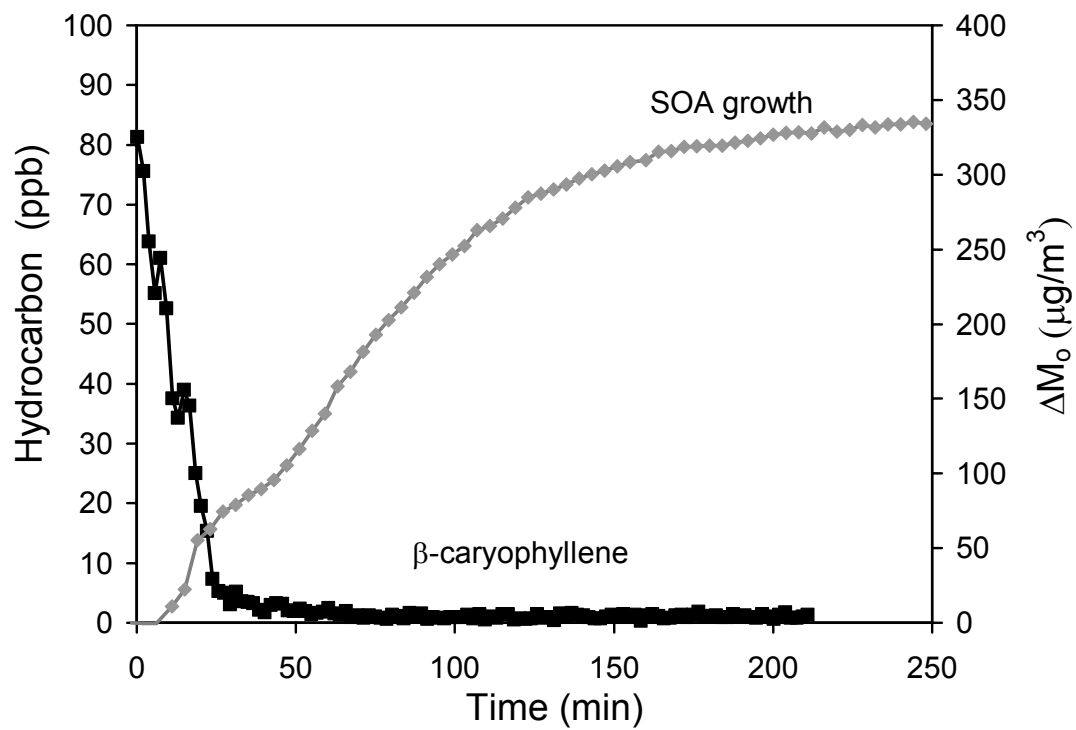
Figure 2. 17.  $\beta$ -caryophyllene ozonolysis and aerosol mass formation

Figure 2. 18.  $\beta$ -caryophyllene and ozone reacted over the course of the experiment (Table 2.2: Experiment on 3/21/2003)

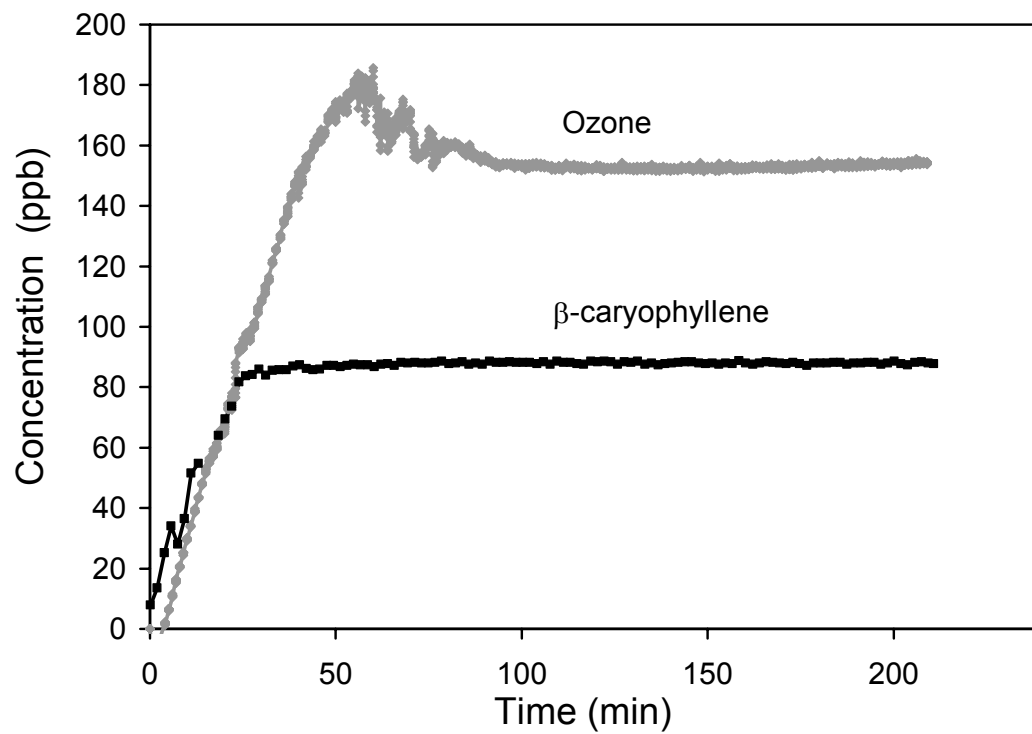


Figure 2. 19. AMS relative delta time series plot for  $\beta$ -caryophyllene ozonolysis. Unsaturated organics yield delta values  $\leq 0$ , and oxygenated organics yield delta values  $\geq 2$ .

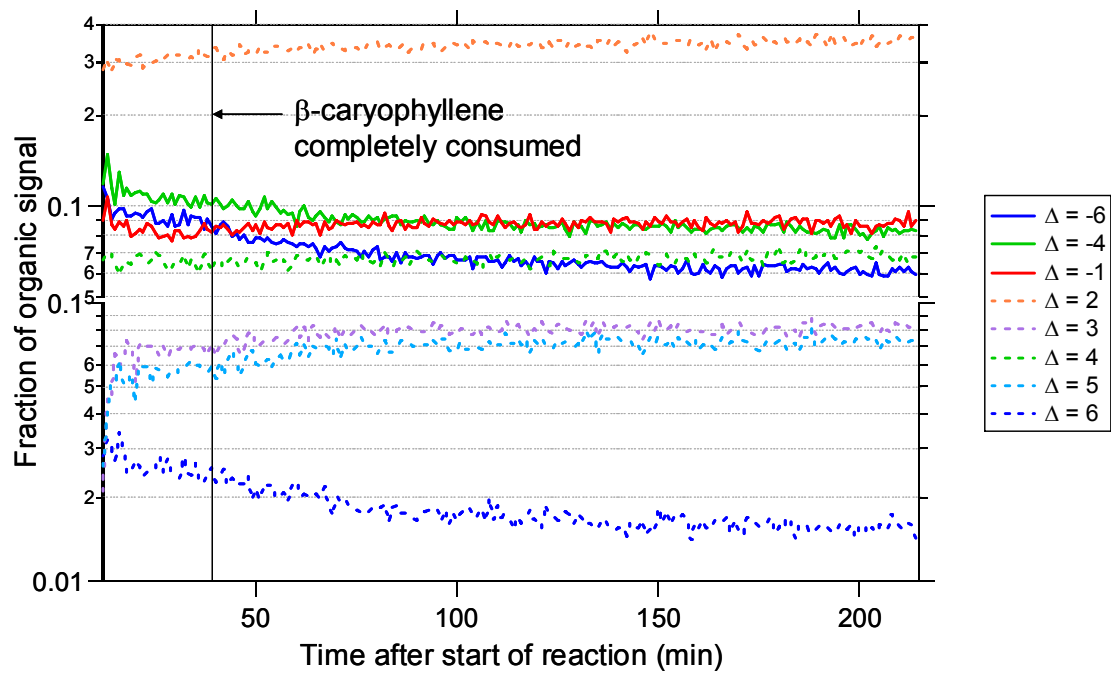




Figure 2. 20. Growth curve for longifolene photooxidation

